Article:
Hu, N, Zhuang, P-Z, Yang, D-S et al. (2021) On the evolution law of a contact normal-based fabric tensor for granular materials. Computers and Geotechnics, 132. 103857. ISSN: 0266-352X

https://doi.org/10.1016/j.compgeo.2020.103857

On the evolution law of a contact normal-based fabric tensor for granular materials

Dr Nian Hu [1, 4]

Email: greaterhu@126.com

Dr Pei-Zhi Zhuang [2,4]

Corresponding author,

Email: zhuangpeizhi@sdu.edu.cn

Dr Dun-Shun Yang [3]

Email: evxdy1@gmail.com

Professor Hai-Sui Yu [5]

Email: h.yu@leeds.ac.uk

1 Nottingham Centre for Geomechanics, Faculty of Engineering, the University of Nottingham, University Park, Nottingham, NG7 2RD, UK

2 School of Qilu Transportation, Shandong University, 250002, Jinan, China.

3 ARUP, 13 Fitzroy St, London, Middlesex W1T 4BQ, UK

4 State Key Laboratory for GeoMechanics and Deep Underground Engineering China University of Mining and Technology, Xuzhou, 221116, China

5 School of Civil Engineering, University of Leeds, Leeds, LS2 9JT, UK

Revision on 15 September 2020

ABSTRACT

This paper presents a theoretical study on a hybrid fabric evolution law for modelling anisotropic behaviour of granular media. In the hybrid evolution law, the rate of a contact normal-based fabric tensor is related to the rates of both stress ratio tensor and plastic strain. Assumptions and principles that were adopted for the development of the fabric evolution law are presented and discussed at first. Its accuracy is then examined by comparing with discrete element modelling (DEM) results under proportional loading and experimental data under complex loading and unloading processes. It is found that fabric evolution at low stress ratios is closely related to the stress-rate driven term of the hybrid law, while the strain-rate driven term dominates at high stress ratios. The hybrid evolution law satisfies the uniqueness requirement of fabric at the critical state by introducing an 'attractor' concept. Overall, fabric evolutions predicted by the hybrid law show a close agreement with DEM simulation results and experimental data.

***Keywords*:** Anisotropy; Fabric evolution; Anisotropic critical state; Granular material;

1. Introduction

The arrangement and organisation of particles and other features of microstructures within a soil mass are usually termed as its *Fabric*. In granular materials, it is associated with various microstructural quantities such as the elongated particle orientation direction, contact normal vectors, branch vectors, and void vectors. It has been widely observed (in both experimental tests [1-8] and numerical simulations [9-21]) that the fabric of granular materials is of anisotropic nature, which may be produced in the process of deposition (i.e. initial anisotropy) and/or upon anisotropic loading (i.e. induced anisotropy). Fabric anisotropy and its evolution may exert significant effects on the strength and deformation properties of discrete granular materials [1, 4, 17, 22-24], for example, the shear strength [20, 25-27], elastic moduli [28], non-coaxial plastic flow [29-32] and dilatancy [10, 33-35]. These behaviours of granular materials are closely associated with the stability and buckling of force chains at a mesoscopic scale and sliding and rolling at contacts, thus governed by the grain-scale structural characteristics and processes. To capture the fabric features, numerous fabric tensors describing the spatial distribution of different microstructural quantities, statistical representation of the microstructural fabric, have been developed in the literature (e.g. reviewed by Li et al. [36]), and many of them have been incorporated into constitutive models for granular materials as essential internal variables [31, 34, 35, 37-45].

Under shearing, the fabric of granular materials may be regarded as unchanged only at a very low level of strain, typically at the order of 10^{-5} [46]. Beyond this level, the material fabric would reorganise as particles slide and roll across each other, namely the fabric evolves during loading. Results of physical tests [1, 3, 5-7, 47, 48] and numerical simulations [13, 15, 49-54] revealed the following characteristics of fabric evolutions under monotonic shear loading:

- The principal directions of the fabric tensor tend to align with those of the stress tensor. As the principal directions of the stresses rotate, the principal axes of the fabric tensor rotate in a manner that they gradually become coaxial with the loading direction at large strain.
- An ultimate fabric state, i.e. the critical state, which is independent of the initial fabric (void ratio and fabric anisotropy), tends to be achieved at large strain, at which influences of the initial state of the fabric are totally erased.

In order to reproduce the observations of fabric during loading, various evolution laws have been proposed, for example, by connecting the rate of a fabric tensor to either stress/elastic

strain rate [38, 44, 55, 56] or plastic strain rate [3, 10, 14, 34, 40, 57, 58]. The former types of fabric evolution laws are broadly categorised as stress-rate driven evolution laws as stresses and elastic strains can be readily related by elastic models, and the latter is named as strain-rate driven evolution laws in this paper. An overview of the commonly used fabric evolution laws refers to the reference of [59]. Due to the lack of quantitative measurements of relevant grain-scale features and processes, the development of early phenomenological fabric evolution laws heavily relied on the stress-strain information at the macro level.

Benefitting from the advancements of non-destructive imaging technologies, such as X-ray computed tomography [1, 7], and particle-based numerical simulation techniques, such as the discrete element method (DEM) [21], the understanding of anisotropic fabric and its evolution in granular materials has been greatly deepened and many fabric evolution laws have been examined, proposed or improved based on observed particle-scale characteristics [9, 31, 34, 59, 60]. Motivated by micromechanical and experimental studies, Li and Dafalias [34] proposed an Anisotropic Critical State Theory (ACST), which represents a milestone in the constitutive modelling of anisotropic fabric for granular media. Hu et al. [31] examined the performance of typical stress-rate driven and strain-rate driven evolution laws of material fabric in constitutive modelling by comparing with DEM simulation results. It was shown that: (a) evolution laws associated with the stress (or elastic strain) rate alone can capture the characteristics of peak strength under monotonic shearing with various loading directions, but they rarely predict a unique anisotropic critical state; (b) on the contrary, fabric evolution laws associated with the plastic strain rate alone tend to give a unique critical value of the fabric tensor, but they cannot capture the characteristics of peak strength easily. The latter issue has also been recognised by Li and Dafalias [34] while modelling the anisotropic fabric of sand with a simple strain-rate driven evolution law. To capture the peak characteristics during fabric evolution, Yang et al. [40], Wang et al. [10] and Zhao and Kruyt [59], among others, made valuable attempts to improve the strain-rate driven evolution laws based on DEM observations as discussed later in this paper. Alternatively, Hu [61] proposed a hybrid fabric evolution law, assuming the evolution of the fabric tensor in granular materials under monotonic shearing is dependent on the rates of both stress ratio and plastic strain. Yuan et al. [9] extended the hybrid evolution law to incorporate the effects of the intermediate stress ratio on the evolution of fabric. In this paper, the assumptions, procedure and principles that were adopted in the development of the hybrid fabric evolution law are elaborated and discussed for the first time. This is followed by comparison and validation analyses of the fabric evolution laws based on direct grain-scale

observation and measurement from DEM simulations and experimental data in the literature.

This paper is outlined as follows. Section 2 defines the fabric tensor and the anisotropic critical state. Sections 3 and 4 introduce and analyse some general types of stress-rate driven and strain-rate driven fabric evolution laws, respectively, according to the requirements of the principle of material frame-indifference together with assumptions of rate-independence and uniqueness of critical fabric tensor. In Section 5, the hybrid fabric evolution law of Hu [61] is presented and briefly discussed. Then the performance of the hybrid evolution laws is examined by comparing with results of DEM simulations and experimental data in Sections 6 and 7, respectively. Finally, some conclusions are drawn in Section 8.

2 Uniqueness of critical state fabric tensor

2.1. Definition of the fabric tensor

Contacts at where particles interact with each other are often regarded as the fundamental fabric information of granular materials [15, 62]. For a granular assembly of N_P particles and N_c contact points, the relative frequency distribution of contact normals $\boldsymbol{n}$ may be described by a probability density function $E(\boldsymbol{n})$. In most cases, it can be truncated [9, 26, 52, 63] as:

$$E(\boldsymbol{n}) = \frac{1}{4\pi}(1 + \boldsymbol{F}\colon \boldsymbol{n}\otimes\boldsymbol{n}) \tag{1}$$

by second-order spherical harmonic series for three-dimensional (3D) materials, or

$$E(\boldsymbol{n}) = \frac{1}{2\pi}(1 + \boldsymbol{F}\colon \boldsymbol{n}\otimes\boldsymbol{n}) \tag{2}$$

by second-order Fourier series for two-dimensional (2D) materials. The symbol $\otimes$ denotes a dyadic product. The traceless tensor $\boldsymbol{F}$ in Eqs. (1) and (2) is known as the second-order fabric tensor of the third kind in terms of unit contact normal [46]. It is used to characterise the fabric anisotropy in this study as it renders to capture the most essential microstructural features that govern the material behaviour with a small number of parameters [33, 62]. Note that higher-order terms are omitted in Eqs. (1) and (2) for simplicity as the contributions of higher-order terms are usually negligible compared to those from the second-order terms in most cases for various loading paths [26, 64]. Practically, the fabric tensor $\boldsymbol{F}$ can be estimated from the second-order tensor $\boldsymbol{N}$ [10, 13, 26, 65] as follows:

$$\boldsymbol{F} = \frac{15}{2}\left(\boldsymbol{N} - \frac{1}{3}\boldsymbol{I}\right) \quad \text{for 3D case} \tag{3}$$

$$\boldsymbol{F} = 4\left(\boldsymbol{N} - \frac{1}{2}\boldsymbol{I}\right) \quad \text{for 2D case} \tag{4}$$

where $\boldsymbol{I}$ denotes the unit second-order tensor; $\boldsymbol{N}$ is a function of the discrete directional contact normals $\boldsymbol{n}$ of a granular assembly as:

$$\boldsymbol{N} = \frac{1}{N_c}\sum_{c\in N_c} \boldsymbol{n}^c \otimes \boldsymbol{n}^c \tag{5}$$

2.2. The fabric tensor at the critical state

In classical critical state theory (CST), granular materials under a monotonic shearing will achieve a critical state characterised by stationary values of stresses and void ratio with an unlimited development of the shear strain [13, 53, 66-68], and the critical state can be fully described by two analytical equations in a three-dimensional space:

$$e = e_c = \Gamma(p) \tag{6a}$$

$$\eta = \eta_c = (q/p)_c = M(b) \tag{6b}$$

where $p = 1/3\ tr(\boldsymbol{\sigma})$ is the mean effective stress; $q = \sqrt{3/2}\,\|\boldsymbol{S}\|$ is the stress deviator where $\boldsymbol{S}$ is the deviatoric stress tensor, and η is the stress ratio. The operator $\|*\|$ denotes the Euclidean norm. The intermediate principal stress ratio b is defined as $(\sigma_2 - \sigma_3)/(\sigma_1 - \sigma_3)$, in which σ_1, σ_2 and σ_3 are the major, intermediate and minor principal stresses respectively. Compressive stresses are treated as positive in this paper. Eq. (6a) assumes that the critical void ratio e_c is only dependent on the mean effective stress p. Eq. (6b) defines that the critical state stress ratio is only dependent on the shear mode (i.e. b value). The function $M(b)$ represents the effect of the shear mode on the critical state friction angle in the π plane.

The kernel of the idea in the CST is that the critical state line is unique for a given soil regardless of the stress paths and the initial conditions. It has been realized that the two conditions of CST (i.e. Eqs. (6a) and (6b)) may be necessary but are not sufficient to maintain the critical state [34, 69, 70]. Considerable microstructural studies revealed that material fabric at the critical state is anisotropic in nature [9, 11, 13, 34, 50, 53, 57]. Accordingly, Li and Dafalias [34] proposed the ACST, enhancing the two CST conditions by a third, i.e. a critical state value of the fabric. Following this concept, one more condition, specifying the fabric tensor at the critical state, is added to secure the sufficiency of reaching and maintaining the critical state. The critical state fabric tensor $\boldsymbol{F}_c$ is assumed to be proportional to the deviatoric stress ratio tensor $\boldsymbol{\eta}$ at the critical state as:

$$\boldsymbol{F}_c = C_F(b)\boldsymbol{\eta}_c = C_F(b)\left(\frac{\boldsymbol{S}}{p}\right)_c \tag{6c}$$

where C_F is a proportional coefficient that is dependent on the b value [9, 13, 16]. According to the definition of the stress ratio in Eq. (6b), we have $\eta = \sqrt{3/2}\,\|\boldsymbol{\eta}\|$. $\boldsymbol{\eta} = \boldsymbol{S}/p$ is the (deviatoric) stress ratio tensor. If we define the deviator of the critical state fabric tensor as $F_{qc} = \sqrt{3/2}\|\boldsymbol{F}_c\| = M_F$, Eq. (7) can be deduced from Eq. (6c) as:

$$M_F = C_F(b)M(b) \tag{7}$$

The additional constraint of Eq. (6c) characterises the anisotropic feature of granular materials at the critical state. The critical state fabric tensor specifies a boundary condition on the evolution of the fabric. In other words, a unique critical state fabric tensor will be achieved during fabric evolution, independent of the initial conditions and the stress path through which the critical state is reached. The deviator of $\boldsymbol{F}_c$ is equal to $C_F(b)M(b)$, varying with the shear mode. These features of the critical state fabric tensor are consistent with DEM simulation findings [9, 10, 13, 17, 31, 49, 53, 71, 72] as will be elucidated later.

3. Stress-rate driven evolution laws

3.1. A general type of stress-rate driven fabric evolution laws

The spatial distribution of contact normals keeps evolving to achieve mobilised strength. Both experimental observations [3, 47, 48] and numerical simulations [18-20] indicated that the distribution of contact normals is closely related to the applied stresses, and the material fabric tends to align with the applied stresses. In micromechanics, the stress tensor can be directly related to a fabric tensor through the stress-force-fabric relationship [20, 64]. According to these findings, Yu [55] proposed a general type of evolution laws in which the rate of the fabric tensor (i.e. $\dot{\boldsymbol{F}}$) was related to the stress tensor $\boldsymbol{\sigma}$ and the stress rate $\dot{\boldsymbol{\sigma}}$ as

$$\dot{\boldsymbol{F}} = \boldsymbol{B}(\boldsymbol{\sigma}, \dot{\boldsymbol{\sigma}}) \tag{8}$$

In this work our attention is restricted to rate-independent material behaviour. The rate-independence requires that the tensor-valued function $\boldsymbol{B}$ is a homogeneous function of degree one in $\dot{\boldsymbol{\sigma}}$. As such, one can obtain a rate-independent form of the evolution law as follows:

$$\dot{\boldsymbol{F}} = \boldsymbol{B}\left(\boldsymbol{\sigma}, \frac{\dot{\sigma}}{\|\dot{\boldsymbol{\sigma}}\|}\right)\|\dot{\boldsymbol{\sigma}}\| \tag{9}$$

More details of the derivation of Eq. (9) refer to Gurtin et al. [73].

3.1.1. Uniqueness of the critical state fabric tensor

At first, we examined whether evolution laws in the form of Eq. (8) are compatible with the condition of Eq. (6c). The answer is *negative*. In rate-independent granular materials, although the fabric tensor predicted by Eq. (8) will be 'saturated' at the critical state, namely it does not develop further with unlimited shear strain, it varies with the initial fabric conditions (explained in detail in Appendix A). In other words, Eq. (8), in which $\dot{\boldsymbol{F}}$ is purely dependent on $\boldsymbol{\sigma}$ and $\dot{\boldsymbol{\sigma}}$, cannot satisfy the requirement of the uniqueness of the critical state fabric tensor for rate-independent media. Therefore, Eq. (8) is not suitable for describing the evolution of fabric tensors near the critical state. Nevertheless, it does not mean that Eq. (8) is not suitable for other situations. In fact, Eq. (8) is able to describe the evolution of fabric tensor under rotational shearing as well as in the case when the stress ratio is below the critical state stress ratio [61].

3.1.2. Requirements of the principle of material frame-indifference

The principle of material frame-indifference requires that the function $\boldsymbol{B}$ must be a tensor-valued isotropic function on both stress rates and stress tensors. This feature of function $\boldsymbol{B}$ is useful to develop evolution laws for internal variables and fabric tensors by using the representation theorem of isotropic functions. According to the representation theorem for a tensor-valued function of two symmetric tensors in a three-dimensional space [74], evolution laws of the fabric tensor, satisfying the form of Eq. (8), can be generally expressed as:

$$\dot{\boldsymbol{F}} = a_0\boldsymbol{I} + a_1\boldsymbol{\sigma} + a_2\boldsymbol{\sigma}^2 + a_3\dot{\boldsymbol{\sigma}} + a_4\dot{\boldsymbol{\sigma}}^2 + a_5(\boldsymbol{\sigma}\dot{\boldsymbol{\sigma}} + \dot{\boldsymbol{\sigma}}\boldsymbol{\sigma}) + a_6(\boldsymbol{\sigma}^2\dot{\boldsymbol{\sigma}} + \dot{\boldsymbol{\sigma}}\boldsymbol{\sigma}^2) + a_7(\boldsymbol{\sigma}\dot{\boldsymbol{\sigma}}^2 + \dot{\boldsymbol{\sigma}}^2\boldsymbol{\sigma}) \tag{10}$$

where $a_k(k = 0, \cdots, 7)$ are scalar-valued functions of basic invariants listed as follows:

- Invariant Group A: $tr(\boldsymbol{\sigma})$, $tr(\boldsymbol{\sigma}^2)$, $tr(\boldsymbol{\sigma}^3)$
- Invariant Group B: $tr(\dot{\boldsymbol{\sigma}})$, $tr(\boldsymbol{\sigma}\dot{\boldsymbol{\sigma}})$, $tr(\boldsymbol{\sigma}^2\dot{\boldsymbol{\sigma}})$
- Invariant Group C: $tr(\dot{\boldsymbol{\sigma}}^2)$, $tr(\dot{\boldsymbol{\sigma}}^3)$, $tr(\boldsymbol{\sigma}\dot{\boldsymbol{\sigma}}^2)$, $tr(\boldsymbol{\sigma}^2\dot{\boldsymbol{\sigma}}^2)$

Although Eq. (10) exactly represents the constraints imposed by the principle of material frame-indifference, it is too general for practical use. In many cases, low-order terms may be of sufficient accuracy, and the constraint imposed by such simplified relations would generally be stronger than the full description of Eq. (10). We give several specific cases in which high-

order terms can be assimilated or dropped in the following subsection.

3.2. Specific cases of Eq. (10)

It is natural to further assume that $\dot{\boldsymbol{F}}$ is linear with $\dot{\boldsymbol{\sigma}}$ as it is the simplest way to satisfy the requirement of rate-independence, i.e. Eq. (9). With the assumption of linearity, Eq. (10) can be simplified as:

$$\dot{\boldsymbol{F}} = a_0\boldsymbol{I} + a_1\boldsymbol{\sigma} + a_2\boldsymbol{\sigma}^2 + a_3\dot{\boldsymbol{\sigma}} + a_5(\boldsymbol{\sigma}\dot{\boldsymbol{\sigma}} + \dot{\boldsymbol{\sigma}}\boldsymbol{\sigma}) + a_6(\boldsymbol{\sigma}^2\dot{\boldsymbol{\sigma}} + \dot{\boldsymbol{\sigma}}\boldsymbol{\sigma}^2) \tag{11}$$

As the fabric tensor $\boldsymbol{F}$ defined in Eq. (3) is traceless, only the deviatoric part of the fabric tensor rate needs to be kept. Hence, Eq. (11) can be expressed more explicitly as:

$$\dot{\boldsymbol{F}} = \big(a_3 tr(\dot{\boldsymbol{\sigma}}) + a_4 tr(\boldsymbol{\sigma}\dot{\boldsymbol{\sigma}}) + a_5 tr(\boldsymbol{\sigma}^2\dot{\boldsymbol{\sigma}})\big)\boldsymbol{S} + \big(a_6 tr(\dot{\boldsymbol{\sigma}}) + a_7 tr(\boldsymbol{\sigma}\dot{\boldsymbol{\sigma}}) + a_8 tr(\boldsymbol{\sigma}^2\dot{\boldsymbol{\sigma}})\big)(\boldsymbol{\sigma}^2)' + a_9\dot{\boldsymbol{s}} + a_{10}(\boldsymbol{\sigma}\dot{\boldsymbol{\sigma}} + \dot{\boldsymbol{\sigma}}\boldsymbol{\sigma})' + a_{11}(\boldsymbol{\sigma}^2\dot{\boldsymbol{\sigma}} + \dot{\boldsymbol{\sigma}}\boldsymbol{\sigma}^2)' \tag{12}$$

where $a_k (k = 3, \cdots, 11)$ are new single scalar-valued functions, which are dependent on Invariant Group A only. $(*)'$ represents deviatoric part of a second-order tensor $*$, i.e. *dev*$(*)$. Obviously, $\dot{\boldsymbol{F}}(\boldsymbol{\sigma}, \dot{\boldsymbol{\sigma}})$ in Eq. (12) is an odd function of the stress rate $\dot{\boldsymbol{\sigma}}$.

3.2.1. Evolution laws for specific loading paths

Under a proportional loading, the direction of deviatoric stresses $\boldsymbol{l}$ remains constant (e.g. for triaxial compression and triaxial extension). By applying the Cayley-Hamilton theorem, Eq. (12) can be equivalently expressed as:

$$\dot{\boldsymbol{F}} = \big(a_3 tr(\dot{\boldsymbol{\sigma}}) + a_4 tr(\boldsymbol{\sigma}\dot{\boldsymbol{\sigma}})\big)\boldsymbol{S} + \big(a_6 tr(\dot{\boldsymbol{\sigma}}) + a_7 tr(\boldsymbol{\sigma}\dot{\boldsymbol{\sigma}})\big)(\boldsymbol{S}^2)' \tag{13}$$

Under a coaxial loading, the principal axes of stresses are fixed (e.g. the true axial shearing). Since the stress tensor and its rate are coaxial, $\dot{\boldsymbol{F}}$ can be equivalently expressed as

$$\dot{\boldsymbol{F}} = \big(a_3 tr(\dot{\boldsymbol{\sigma}}) + a_4 tr(\boldsymbol{\sigma}\dot{\boldsymbol{\sigma}}) + a_5 tr(\boldsymbol{\sigma}^2\dot{\boldsymbol{\sigma}})\big)\boldsymbol{S} + \big(a_6 tr(\dot{\boldsymbol{\sigma}}) + a_7 tr(\boldsymbol{\sigma}\dot{\boldsymbol{\sigma}}) + a_8 tr(\boldsymbol{\sigma}^2\dot{\boldsymbol{\sigma}})\big)(\boldsymbol{S}^2)' \tag{14}$$

Under a purely rotational shearing where the principal axes rotate but all stress invariants are kept constant, the rate of stress tensor and the stress tensor satisfy the following equations:

$$tr(\dot{\boldsymbol{\sigma}}) = 0; \;\; tr(\dot{\boldsymbol{\sigma}}\boldsymbol{\sigma}) = 0; \;\; tr(\dot{\boldsymbol{\sigma}}\boldsymbol{\sigma}^2) = 0 \tag{15}$$

Combining Eq. (18) with Eq. (15) leads to:

$$\dot{\boldsymbol{F}} = \left(a_9\dot{\boldsymbol{S}} + a_{10}\left(\boldsymbol{S}\dot{\boldsymbol{S}} + \dot{\boldsymbol{S}}\boldsymbol{S}\right) + a_{11}\left(\boldsymbol{S}^2\dot{\boldsymbol{S}} + \dot{\boldsymbol{S}}\boldsymbol{S}^2\right)\right)' \tag{16}$$

The above example cases clearly show that different terms in Eq. (12) represent the effects of different components of the stress tensor and the stress rate on fabric evolution. According to the problem of stress paths in hand, specific forms of the stress-rate driven fabric evolution law can be obtained by tailoring the terms in Eq. (12).

3.2.2. A simple evolution law for proportional loading

According to the DEM simulation results of tests under proportional loading by Yang [51], which showed the second invariant of fabric tensor $F_q = \sqrt{3/2}\|\boldsymbol{F}\|$ varied non-linearly with the stress ratio η, a simple non-linear evolution law is proposed in Eq. (17) as:

$$\dot{\boldsymbol{F}} = C_1(1 + C_2\|\boldsymbol{\eta}\|)\dot{\boldsymbol{\eta}} = C_1(1 + C_2\|\boldsymbol{\eta}\|)\left(\frac{\dot{\boldsymbol{S}}}{p} - \frac{\boldsymbol{S}}{p^2}\dot{p}\right) \tag{17}$$

where C_1 and C_2 are material constants controlling the pace of fabric evolution. Note that Eq. (17) is a special case of Eq. (12) while designating:

$$a_3 = -\frac{C_1(1+C_2\|\boldsymbol{\eta}\|)}{3p^2};\ \ a_9 = \frac{C_1(1+C_2\|\boldsymbol{\eta}\|)}{p};\ \ a_{k(k\neq 3,9)} = 0 \tag{18}$$

In Eq. (18), two terms of Eq. (12) are kept. In this simple evolution law, the rate of the fabric tensor is assumed to be proportional to the rate of stress ratio tensor. Setting $C_2 = 0$, Eq. (17) reduces to the fabric evolution law proposed by Wan and Guo [38], that is:

$$\dot{\boldsymbol{F}} = C_1\dot{\boldsymbol{\eta}} \tag{19}$$

Eq. (19) relates the rate of the fabric tensor to the rate of the stress ratio. It predicts that the fabric tensor stops evolving at the critical state as the stress ratio 'saturated' [38]. Integrating Eq. (19) under a proportional loading leads to a linear relation between $||\boldsymbol{F}|$ and $||\boldsymbol{\eta}||$ from an initial isotropic fabric tensor. This disadvantage is eliminated by Eq. (17).

Satake [65] assumed that the fabric tensor is proportional to the stress tensor normalised by the mean effective stress, i.e.

$$\dot{\boldsymbol{F}} = C_1(\dot{\boldsymbol{\sigma}}/p) = C_1(\frac{\dot{\boldsymbol{\sigma}}}{p} - \frac{\boldsymbol{\sigma}}{p^2}\dot{p}) = C_1(\frac{\dot{\boldsymbol{S}}}{p} - \frac{\boldsymbol{S}}{p^2}\dot{p}) \tag{20}$$

This evolution law is essentially identical to that of Eq. (19). The dependence of the fabric tensor on the stress rate has been observed in physical tests [47, 48], in which the distribution

of contact normals was closely related to the applied stresses (e.g. Eqs. (19) and (20)). It has also been argued that the fabric evolution depends on the elastic rate of deformation rather than the plastic rate of deformation as they presumed that only the elastic deformation gives rise to a change in stresses and causes distortion of the fabric [44, 56]. However, this is not necessarily true as many recent studies [9, 10, 31, 34] showed that the fabric evolution may also closely associate with the development of plastic strains prior to the critical state.

4. Strain-rate driven evolution laws

Strain-rate driven type of evolution laws were initially proposed to describe kinematic hardening of internal state (hardening) parameters for metals (e.g. [75]) and then applied to describe the rotational hardening of soils (e.g. [76-78]). Based on some existing fabric evolution laws for granular materials in the literature (e.g. [3, 14, 34, 40, 57, 58]), a general type of the strain-rate driven evolution laws is given at first in Eq.(21).

$$\dot{\boldsymbol{F}} = C_1 a(\boldsymbol{\sigma}, \boldsymbol{F})(\boldsymbol{B}(\boldsymbol{\sigma}, \boldsymbol{F}) - \boldsymbol{F})\dot{\Lambda} \tag{21}$$

where C_1 is a material constant controlling the pace of fabric evolution; $\dot{\Lambda}$ is a plastic index defined as the norm of deviatoric plastic strain rates, i.e. $\dot{\Lambda} = \left\| \dot{\boldsymbol{e}}_p \right\|$; $a(\boldsymbol{\sigma}, \boldsymbol{F})$ is a positive isotropic scalar-valued function of the stress tensor $\boldsymbol{\sigma}$ and the fabric tensor $\boldsymbol{F}$; $\boldsymbol{B}(\boldsymbol{\sigma}, \boldsymbol{F})$ is an isotropic tensor-valued function. Eq. (21) meets the requirement of the principle of material frame-indifference as both $a(\boldsymbol{\sigma}, \boldsymbol{F})$ and $\boldsymbol{B}(\boldsymbol{\sigma}, \boldsymbol{F})$ are isotropic functions, and it is also compatible with the assumption of rate-independence according to the definition of $\dot{\Lambda}$.

4.1. Uniqueness of the critical state fabric tensor

Taiebat and Dafalias [76] introduced an 'attractor' concept to ensure that the anisotropic state parameter, which macroscopically reflects material anisotropy, will reach and rest on the pre-defined limit surface (normally in the stress spaces) under continuously monotonic shearing. Following this concept, we proposed a general attractor in the form of $\boldsymbol{B}(\boldsymbol{\sigma}, \boldsymbol{F}) - \boldsymbol{F}$ in Eq. (21), which implies a relationship between the critical state fabric tensor and the stress tensor and ensures a unique critical state fabric tensor. Specifically, the plastic index $\dot{\Lambda}$ in Eq. (21) is always positive under monotonic shearing, hence the rate of evolution of the fabric tensor reduces to be zero when the attractor $(\boldsymbol{B}(\boldsymbol{\sigma}, \boldsymbol{F}) - \boldsymbol{F})$ approaches zero at the critical state. During shearing, the fabric tensor evolves towards the fixed point that is defined in Eq. (22).

$$\boldsymbol{B}(\boldsymbol{\sigma}_c, \boldsymbol{F}_c) - \boldsymbol{F}_c = \boldsymbol{0} \tag{22}$$

where $\boldsymbol{\sigma}_c$ and $\boldsymbol{F}_c$ represent the critical state stress and fabric tensors, respectively. Eqs. (21) and (22) specify that the fabric tensor may evolve from an arbitrary initial value of $\boldsymbol{F}_i$ towards the critical state fabric tensor $\boldsymbol{F}_c$, and $\boldsymbol{F}_c$ will stay the same with further development of plastic strains. According to the representative theorem of isotropic tensor-valued function, it is found that $\boldsymbol{F}_c$ must be coaxial with $\boldsymbol{\sigma}_c$ as $\boldsymbol{B}$ is an isotropic tensor-valued function of them.

Following Eqs. (6c) and (22), various forms of the function $\boldsymbol{B}$ can be specified, for example:

$$\boldsymbol{B}(\boldsymbol{\sigma},\boldsymbol{F}) = C_F(b)\boldsymbol{\eta} \tag{23a}$$

$$\boldsymbol{B}(\boldsymbol{\sigma},\boldsymbol{F}) = M_F(b)\boldsymbol{n};\ \ \boldsymbol{n} = \frac{\boldsymbol{\eta}}{\|\boldsymbol{\eta}\|};\ \ \boldsymbol{n}:\boldsymbol{n} = 1 \tag{23b}$$

$$\boldsymbol{B}(\boldsymbol{\sigma},\boldsymbol{F}) = M_F(b)\boldsymbol{n};\ \ \boldsymbol{n} = \frac{\boldsymbol{\eta}-\boldsymbol{F}}{\|\boldsymbol{\eta}-\boldsymbol{F}\|};\ \ \boldsymbol{n}:\boldsymbol{n} = 1 \tag{23c}$$

Note that, although the above $\boldsymbol{B}$ functions are all compatible with Eq. (6c) at the critical state, they define different paces of fabric evolution towards the critical state. The 'attractor' concept here may be explained from different perspectives. According to Ma and Zhang [79] and Kuhn [80], the evolution of contact normals in granular assembly can be treated as transport phenomena. At grain scales, the movement of the contacts is characterized by the generation, disruption, convection and diffusion of contact normals on a unit sphere. Correspondingly, the evolution of the spatial distribution of contact normals is governed by Fokker-Planck equations on a unit sphere including source, convective and diffuse terms. Under monotonic shearing, the fabric evolves towards the critical state that corresponds to the steady state of the Fokker-Planck equations. The attractor is a similar description of the evolution of Fokker-Planck equations towards the critical state in the form of fabric tensor. At a meso-scale, the existence of an attractor is closely associated with the fact that the buckling of the force chain cannot continue unlimitedly. During monotonic shearing, especially after the peak, the force chain is in a metastable state and the force network evolves towards a 'dynamic' equilibrium state.

4.2. A simple strain-rate driven evolution law

If we choose $a(\boldsymbol{\sigma},\boldsymbol{F}) = 1$ and $\boldsymbol{B}(\boldsymbol{\sigma},\boldsymbol{F})$ in the form of Eq. (23a) and assume that $C_F(b)$ is independent of the b value for simplicity, a simple evolution law is obtained from Eq. (21) as:

$$\dot{\boldsymbol{F}} = C_1(C_F\boldsymbol{\eta} - \boldsymbol{F})\dot{\Lambda} \tag{24}$$

This is similar to the evolution law that was proposed by Li and Dafalias [34] (i.e. Eq. (25)), in which a traceless void vector-based fabric tensor $\boldsymbol{n}_l$ was used.

$$\dot{\boldsymbol{F}} = C_c(\boldsymbol{n}_l - r\boldsymbol{F})\dot{\Lambda};\ \ \boldsymbol{n}_l{:}\boldsymbol{n}_l = 1 \tag{25}$$

where $\boldsymbol{n}_l$ represents a direction along which the loading is applied. C_c and r dictate the pace of fabric evolution and its peak value, respectively.

The critical state fabric tensor $\boldsymbol{F}$ in Eq. (25) is normalised by its norm $\|\boldsymbol{F}_c\|$ and hence there always is $\boldsymbol{F}_c{:}\boldsymbol{F}_c = 1$. Instead, the contact normal based-fabric tensor is attracted by $C_F\boldsymbol{\eta}$ in Eq. (24) so that the deviator of the critical state fabric tensor can be defined simultaneously (e.g. Eqs. (6c) and (7)). $r = 1$ was assumed by Li and Dafalias [34] for simplicity in the constitutive formulation with Eq. (25). In this case, this evolution law can be recovered by using a $\boldsymbol{B}(\boldsymbol{\sigma}, \boldsymbol{F})$ function in the form of Eq. (26c). However, Li and Dafalias [34] noticed that this simplification is not able to capture the peak characteristics of the deviator of the fabric tensor in dense sand. Instead of being constant, r should be able to evolve nonlinearly, whose value is smaller than the unity before reaching the critical state and equals 1 at the critical state. For this reason, Yang et al. [40] incorporated the material dilatancy into the evolution of r; Wang et al. [10] related r to the evolution of the particle orientation fabric tensor. Similarly, Zhao and Kruyt [59] related the coefficient of $\dot{\Lambda}$ with a nonlinear function of the state parameter for modelling the peak characteristics of fabric evolution.

5. The hybrid fabric evolution law of Hu [61]

In order to avoid the aforementioned limitations existing in purely stress-rate driven and simple strain-rate driven evaluation laws, Hu [61] proposed to combine Eqs. (17) and (24) for characterising fabric evolution of granular materials under proportional loading. By doing so, the rate of the fabric tensor is related to the rates of both stress ratio and plastic strain as:

$$\dot{\boldsymbol{F}} = C_1(1 + C_2\|\boldsymbol{\eta}\|)\dot{\boldsymbol{\eta}} + C_3(C_4\boldsymbol{\eta} - \boldsymbol{F})\dot{\Lambda} \tag{26}$$

Comparing to Eqs. (17) and (24), two additional material parameters are involved in Eq. (26). Eq. (26) satisfies both the uniqueness requirement of the fabric tensor at the critical state and the requirement of the principle of material frame-indifference as Eqs. (17) and (24) do. Based on the stress-force-fabric relationship in micromechanics, the fabric tensor can be incorporated into a yield surface through the concept of back stress [42, 55]. As a result, fabric evolutions predicted by Eq. (26) will result in rotational hardening of the yield surface, which will be 'saturated' at a unique critical state [31]. This suggests that the rotational hardening law, widely used in constitutive modelling of granular materials [77, 81], phenomenally represents the

fabric evolution at the grain scale [43]. Moreover, the incorporation of the fabric evolution in the plastic flow rule will lead to non-coaxial plastic deformation as the fabric tensor is generally not coincident with the stress tensor [31, 35].

The first (stress rate) and second (strain rate) terms in Eq. (26) may be associated with different microscopic mechanisms of fabric evolution [9, 31]. At the initial stage of shearing with rapid increases in the stress ratio, contacts are forced to reorganise to support the applied stresses. The change of distribution of contact normals, hence the evolution of the fabric tensor, is mainly due to the net creation of the contacts. At this stage, the plastic strain rate is relatively small, the fabric evolution can thus be effectively related to the stress ratio rate as expressed in the first term of Eq. (26). As shearing continues (especially after the peak strength), the net rate of contact creation decreases considerably, and the change of the contact normal distribution is predominantly controlled by the migration of contact points through sliding and rolling of particles across each other, accompanied by rapid increases of plastic deformation. Hence, the fabric evolution can be effectively related to the plastic strain rate at large shear strains [14, 28] as approximated by the second term of Eq. (26), which ensures that the fabric tensor evolves towards a unique critical state.

6. Performances of fabric evolution laws under proportional monotonic shearing

This section examines the performance of the hybrid fabric evolution law (i.e. Eq. (26)) under monotonic shearing with constant mean stress p and b value. The predicted fabric evolutions are compared with the DEM simulation results obtained by Yang [51]. In the meanwhile, individual influences of the stress-rate driven term (i.e. setting $C_3 = 0$ and $C_4 = 0$ in Eq. (26)) and the strain-rate driven term (i.e. setting $C_1 = 0$ and $C_2 = 0$ in Eq. (26)) of the hybrid law on the evolution of material fabric are also discussed.

6.1 DEM model

The DEM simulations were performed using the commercial package of PFC^{3D} (2004). Non-spherical particles (clumps) were used, which were formed by two identical and overlapping spheres. The distance between two spheres in a clump was 1.4 times of the radius of each sphere R_s, and R_s randomly distributed in the range of 0.3 mm and 0.5 mm. The local contact behaviour was described by the linear contact model. Sliding occurs when the tangential contact force exceeds the maximum allowable tangential force F_{max}^t ($F_{max}^t = \mu F_n^t$, where μ is

the frictional coefficient and F_n^t is the normal stress at contacts). Contact cohesion and crushing mechanism have not been considered. The model parameters used are summarised in Table .

Table 1 DEM simulation details

Particle solid density ρ	Normal stiffness for sphere k_n	Tangential stiffness for sphere k_s	Friction coefficient for sphere μ	Time-step Δt	Damping coefficient ξ
2700kg/m^3	1×10^5 N/m	1×10^5 N/m	0.5	1.02×10^{-6} s	0.7

Initially, anisotropic samples of non-spherical particles were generated by the gravitational deposition method in a cubic box of dimensions of 0.0912m×0.0912m×0.133m. After the deposition process, the polyhedral boundary walls were generated by selecting n=8 and R_w= 0.0066m, where n is the number of sides of the top regular polygon wall surface and R_w is the radius of the polyhedron inscribed sphere. The boundary surfaces were rigid walls with the same mechanical properties as the granular particles. More details about the polyhedral specimen refer to references of [51] and [82]. Each specimen consisted of 5188 particles, and Yang [51] verified that the number of particles is great enough to serve as a representative volume element using the polyhedral specimen. Afterwards, the anisotropic samples were sheared to the deviatoric strain of 10% under triaxial compression, followed by unloading to the isotropic stress state (see Fig. 1). The pre-loaded dense samples (i.e. No. CDED_TC_TT in [51]) had an initial void ratio e_0 of 0.65. Finally, true triaxial tests were performed on the samples. During the monotonic shearing, the mean stress p was kept as constant at 500kPa and $b = 0.4$; the direction of the major principal stress was fixed at different angles to the deposition direction, ranging from 0° to 90° at an interval of 15° (see Fig. 1a).

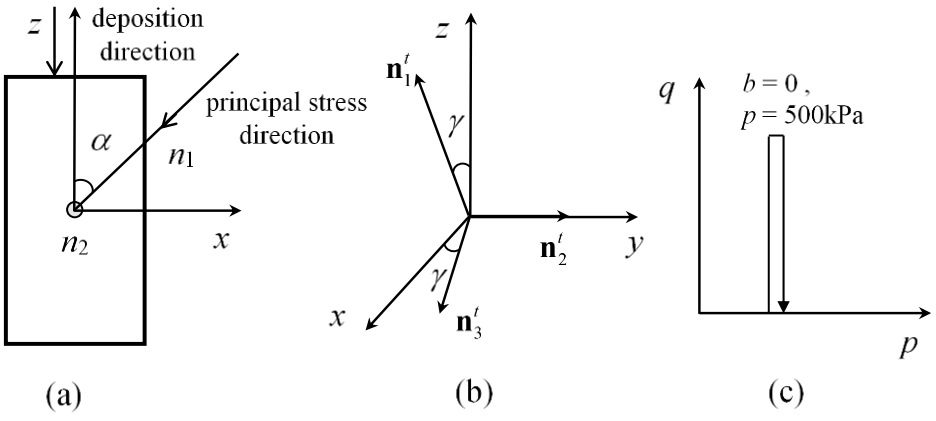

Fig. 1 (a) Definition of loading direction; (b) Definition of principal fabric direction; (c) Loading history of the pre-sheared DEM samples.

The fabric tensor can be fully characterised by the fabric deviator $F_q = \sqrt{3/2}\|\boldsymbol{F}\|$, the intermediate fabric ratio $F_b = (F_1 - F_2)/(F_1 - F_3)$ (where F_1, F_2 and F_3 are the major, intermediate and minor principal values of the fabric tensor respectively) and the major principal direction of the fabric tensor γ_F (see Fig. 1b). The initial fabric before the monotonic shearing in the DEM tests was characterised as $F_{qi} = 0.72,\ F_{bi} = 0.0192,\ \gamma_{Fi} = 0^{\circ}$. The critical state stress ratio η_c was equal to 0.95, and the critical state fabric deviator $F_{qc} = 1$.

6.2 Comparison with DEM simulation results

Model parameters required by the hybrid evolution law are summarized in Table 2, which were calibrated by fitting results of the DEM simulations. The evolution laws were integrated using an implicit Euler algorithm [9, 61] with values of the stress tensor and the strain tensor that were obtained from the DEM tests. Note that $\dot{\Lambda}$ was calculated using the total strain rate as the elastic strain rate is negligibly small compared with the plastic strain rate.

Table 2Model parameters for the hybrid fabric evolution law

Evolution law	Parameters			
	C_1*	C_2	C_3	C_4*
Eq. (26)	0.32	1.3	9	1/0.95

* Note that C_1 and C_4 may be dependent on the b value [9]. As the b value was set as constant in the DEM simulations under monotonic shearing, they were set as constant accordingly here.

Figs. 2 and 3 compared fabric deviators obtained from the DEM simulations and theoretical predictions, plotted against stress ratio η and deviatoric strain ε_q, respectively. Simulation results in Fig. 2 (a) show that before reaching the peak strength, there is a non-linear functional relationship between the stress ratio and the fabric deviator as also observed in experimental investigations [47]. After the peak strength, the fabric deviator evolves with the stress ratio in a totally different manner. For tests performed under different loading directions, F_q evolves consistently towards a unique critical value with increasing strains (e.g. Fig. 3(a)). Figs. 4 and 5 present simulated and predicted evolutions of F_b and γ_F respectively, plotted against stress ratio. The DEM simulation results show that the fabric tensor (i.e. the value of F_b) tends to have the same b value and be coaxial with the stress tensor towards the critical state, as what we have assumed for the critical state fabric tensor in Eq. (6c). The comparisons indicate that the above features of fabric evolution can be well captured by the hybrid evolution law although the predicted peace to reach the critical state is slightly quicker than the DEM measurements.

At low stress ratios (or small shear strains), the material is more likely to behave elastically. Figs. 2-5 indicate that, with a stress ratio up to 0.6, the fabric evolution is closely related to the stress-rate driven term of Eq. (26). This is in line with experimental observations in which the fabric evolution shows a strong link with the stress ratio and the material fabric attempts to align with stresses [47, 83]. Beyond this stage, Eq. (26) is no longer suitable for predicting the fabric evolution if only the stress-rate driven term is involved, particularly at the post-peak stage. For example, the purely stress-rate driven term predicted the $\eta - F_q$ curves in the softening regime return exactly along the paths they came along (i.e. η varies from the peak value η_p to the critical state value η_c) (see Fig. 2(b)), the critical state fabric deviators are different in loading directions (see Fig. 3(b)), and the principal direction of the fabric only rotates a small angle (see Fig. 5(b). All these features are against the DEM observations (e.g. Figs. 2(a) and 3(a)). Those findings also echoed the conclusion made in Section 3.1.1 that the purely stress-rate driven evolution laws cannot warrant a unique critical state fabric tensor.

At higher stress ratios (or larger shear strains), the fabric evolution tends to be more related to the (plastic) strain-rate driven term of Eq. (26) as the material becomes more likely in the plastic state. By introducing the 'attractor' concept, a unique critical state is predicted, and this is consistent with the DEM results (Figs. 2(c, d) and 3(c, d)). Nevertheless, Figs. 2-5 shows that, if excluding the stress-state term, Eq. (26) becomes much less accurate at low stress ratios, especially for tests at small loading angles (e.g. $\alpha = 0^o$), compared to the DEM results. The evolution of fabric in the entire range of stress ratios can be well reproduced by the hybrid law that incorporates both a stress-rate driven term and a strain-rate driven term. It may be assumed that, when the granular material transits from an elastic state to plasticity under monotonic shearing, that governs the fabric evolution gradually transfers from the stress-rate driven term to the plastic-strain-rate driven term in Eq. (26).

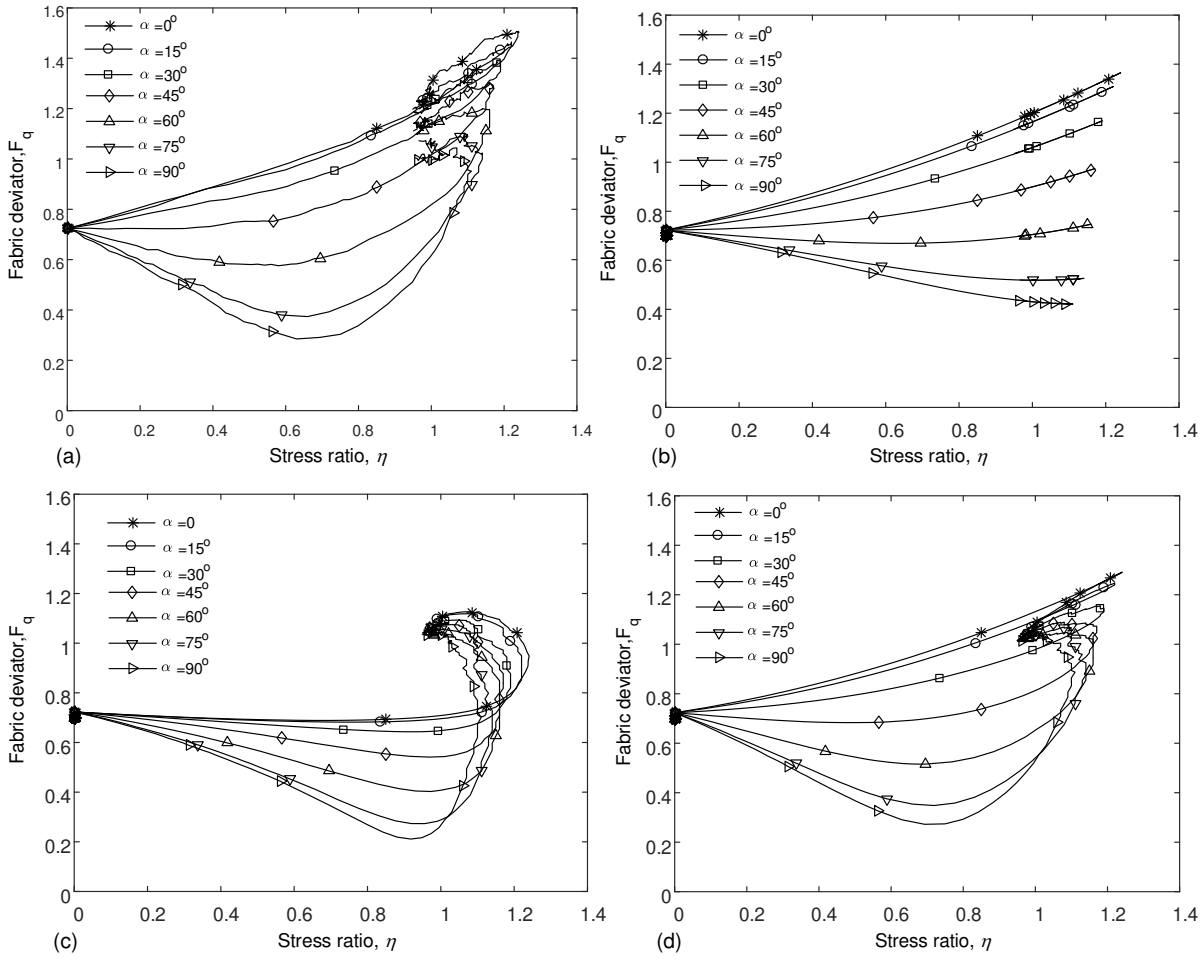

Fig. 2 Simulated and predicted fabric evolution: stress ratio η vs. fabric deviator F_q. (a) DEM; (b) Stress-rate driven term of Eq. (26); (c) Strain-rate driven term of Eq. (26); (d) Eq. (26).

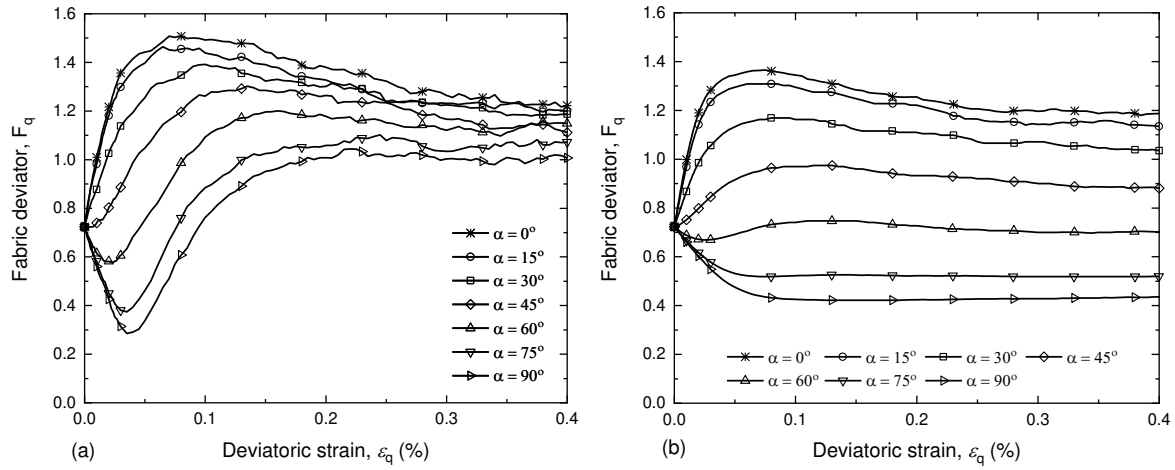

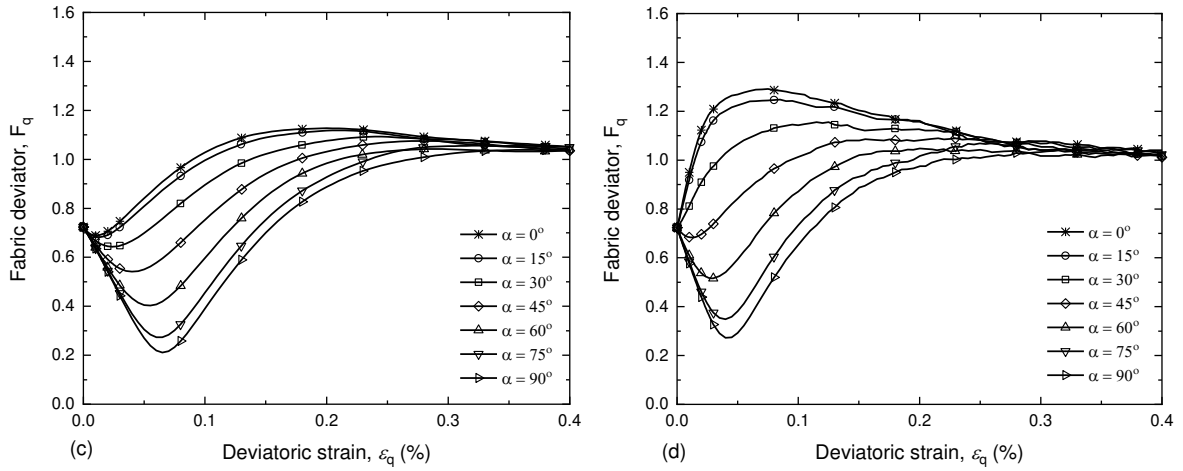

427

428 Fig. 3 Simulated and predicted fabric evolution: deviatoric strain ε_q vs. fabric deviator F_q. (a)
429 DEM; (b) Stress-rate driven term of Eq. (26); (c) Strain-rate driven term of Eq. (26); (d) Eq.
430 (26).

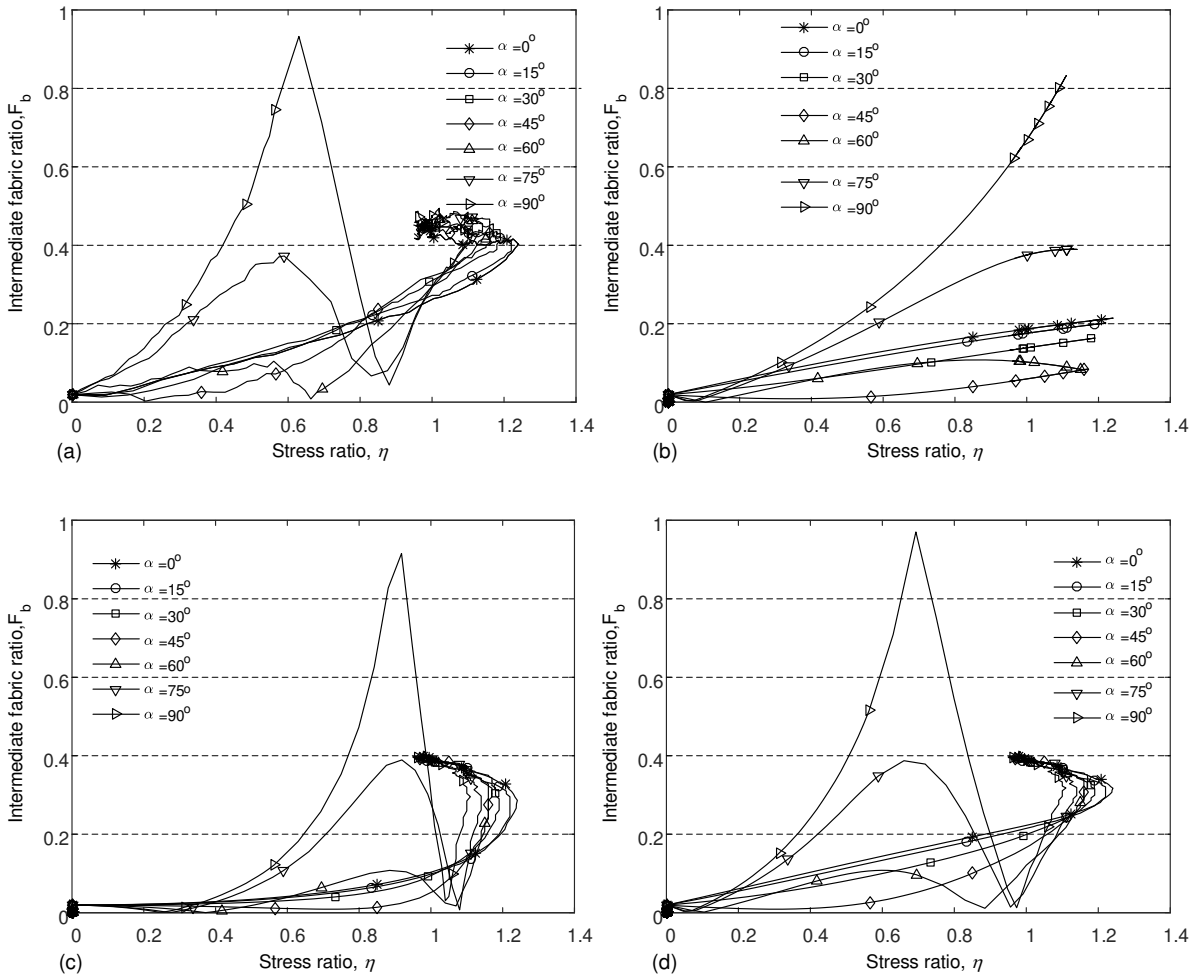

431

432

433 Fig. 4 Simulated and predicted fabric evolution: stress ratio η vs. intermediate fabric ratio F_b.
434 (a) DEM; (b) Stress-rate driven term of Eq. (26); (c) Strain-rate driven term of Eq. (26); (d)
435 Eq. (26).

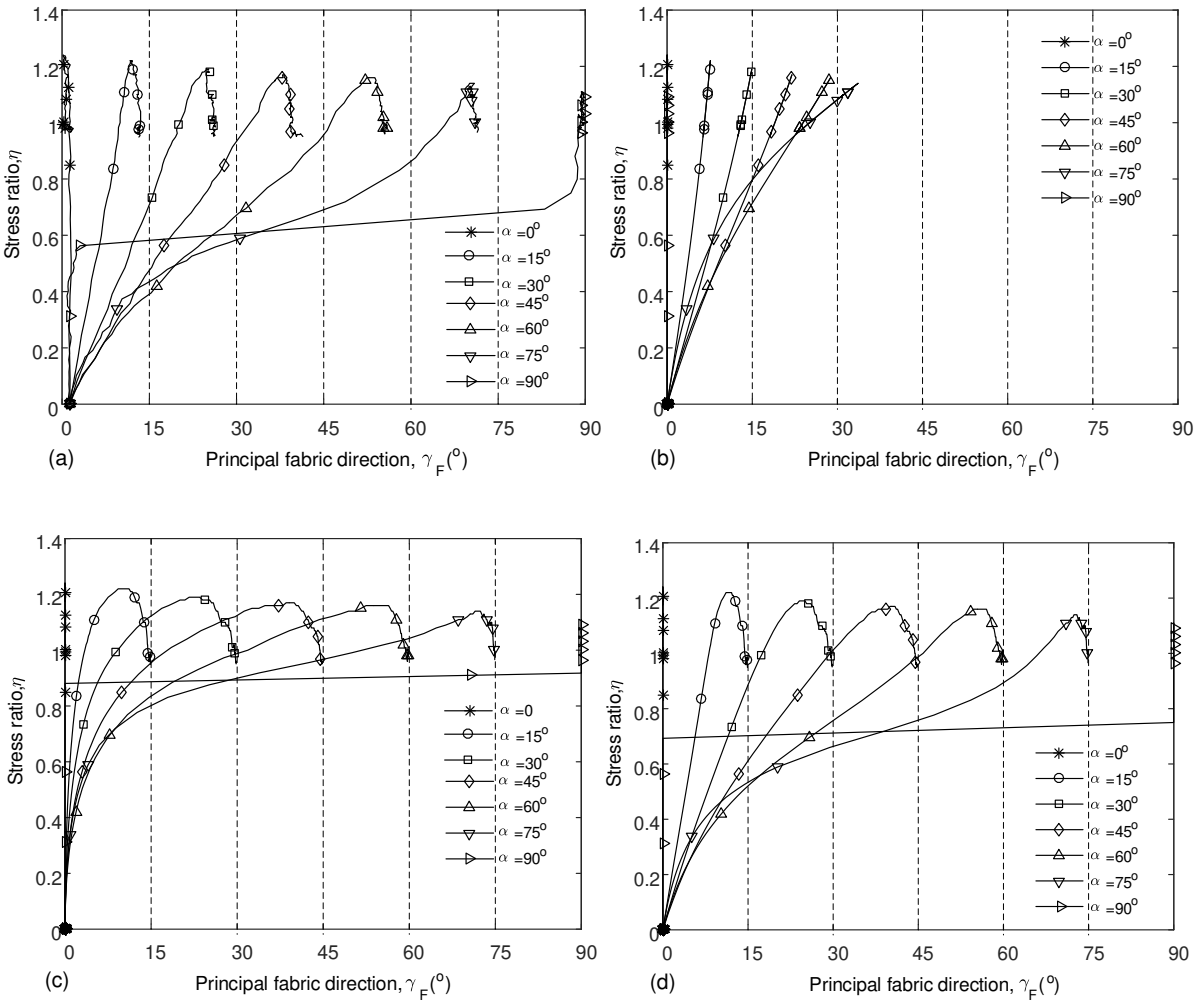

Fig. 5 Simulated and predicted fabric evolution under proportional loading: principal fabric direction γ_F vs. stress ratio η. (a) DEM; (b) Stress-rate driven term of Eq. (26); (c) Strain-rate driven term of Eq. (26); (d) Eq. (26).

7. Comparison with experimental tests

The hybrid evolution law is further compared against experimental data in the literature to examine its accuracy in describing the evolution of fabric tensors. As contact normals of granular materials under three dimensional (3D) conditions were rarely detected in physical tests at this moment, test results on samples made of 2D (Schneebeli) granular materials were used here. The sample types and model parameters involved in the validation are listed in Table 2. Like the 3D cases, notations for the 2D cases are defined as follows.

$$p = tr(\boldsymbol{\sigma})/2\,;\quad \boldsymbol{S} = \boldsymbol{\sigma} - p\boldsymbol{I};\quad \boldsymbol{\eta} = \frac{\boldsymbol{S}}{p} \tag{27}$$

where $p, \boldsymbol{S}$ and $\boldsymbol{\eta}$ are the mean effective stress, the deviatoric stress, and the stress ratio tensor,

450 respectively.

451 $$\eta = \|\boldsymbol{\eta}\|;\ \ \varepsilon_q = \|\boldsymbol{e}_p\|;\ \ \dot{\Lambda} = \|\dot{\boldsymbol{e}}_p\|;\ \ F_q = \|\boldsymbol{F}\|;\ \ \tan(2\gamma_F) = \frac{2F_{21}}{F_{22}-F_{11}} \quad (28)$$

452 where η, ε_q, $\dot{\Lambda}$, F_q and γ_F are the stress ratio, the plastic strain deviator, the plastic index, the
453 fabric deviator and the major principal direction of fabric tensors with respect to the axis 2,
454 respectively. In the 2D case, the fabric tensor can be completely expressed by the fabric
455 deviator F_q and the major principal direction of the fabric tensor, γ_F, as the fabric tensor is
456 traceless. The fabric deviator characterises the degree of concentration of contact normals in
457 preferred directions, i.e. γ_F. Note that the elastic strain was ignored while calculating the plastic
458 index in the following model predictions.

459 Table 1 Test samples, loading types and model parameters.

No.	Materials	Test type	Model parameters				Reference
			C_1	C_2	C_3	C_4	
1	Polydisperse oval photoelastic rods	Biaxial compression	0.35	0.13	3	1	Oda et al. [4]
2*	Polydisperse circular wooden rods	CHCV1	0.1	0	10	1.2	Calvetti et al. [3]
		UVUH1					
		UDUG1					
		CHCD1					

460 ** V represents vertical compression; H represents horizontal compression; D and G represent*
461 *right shear and left shear respectively; C is used for tests with constant normal stress; and U*
462 *is used for constant volume tests. For instance, CHCD1 is a test in which the specimen is first*
463 *loaded in horizontal compression (H) ($\dot{\varepsilon}_x$=constant) under constant vertical stress (C), and*
464 *then subjected to right shear (D) ($\dot{\gamma}$=constant > 0) under constant vertical stress (C).*

465 *7.1. Comparison with tests of Oda et al. [4]*

466 Biaxial compression tests were performed on 2D assemblies of oval cross-sectional rods
467 (polyurethane rubber) by Oda et al. [4]. The photoelastically sensitive rods were lubricated,
468 leading to the interparticle friction angle was about 26°. As a result, the internal friction angles
469 of the assemblies are comparable to those of natural sands [47]. The assemblies were tilted and
470 held at a desired angle α (so-called the bedding angle) in the frame, followed by stacking the
471 rod-like particles by hand with the long axes of their cross-section horizontally. After the
472 completion of the assembly, the frame was brought back (see Fig. 6). A series of assemblies
473 with different bedding angles, i.e. initial fabrics, were tested. The assemblies were sheared by
474 increasing the vertical displacement incrementally with a constant lateral force. The contact
475 normals and their evolution for the assembly of $\alpha = 0^{\circ}$ and 60° were measured, respectively.

More details of the tests refer to [22]. Noted that the second-order fabric tensor of the second kind in terms of unit contact normal [63] that was used by Oda et al. [4] was converted to the fabric tensor defined in this paper (i.e., Eq. (4)) for direct comparison.

Figs. 6 and 7 present measured and predicted results of fabric evolutions for assemblies with different initial fabrics in terms of fabric deviator and major principal fabric direction, respectively. Under displacement-controlled biaxial compression, the fabric anisotropy, represented by the fabric deviator, increases with the development of shear strains until a peak value is reached, responding to the increase in the stress ratio, then drops with decreases in the stress ratio (Fig. 6). The principal axes of the fabric tensor rotated gradually towards the principal axes of the stress tensor regardless of the initial fabric tensor being coaxial or non-coaxial with the stress tensor (Fig. 7). The comparison results indicate that the above features of fabric evolution under biaxial compression for assemblies with different initial fabrics can be well reproduced by the present hybrid evolution law.

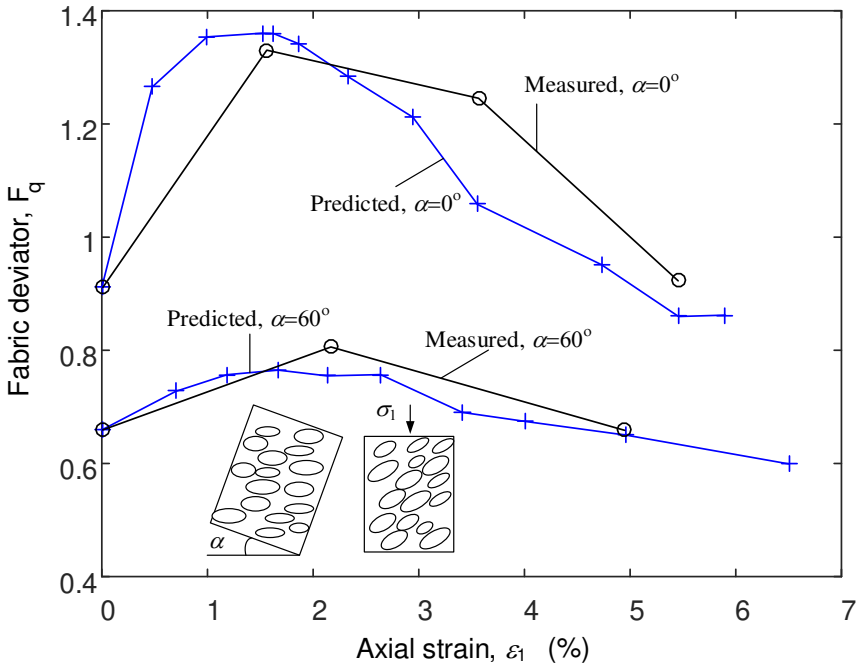

Fig. 6 Measured and predicted evolutions of the fabric deviator F_q with axial strain ε_1 for assemblies with different initial fabrics.

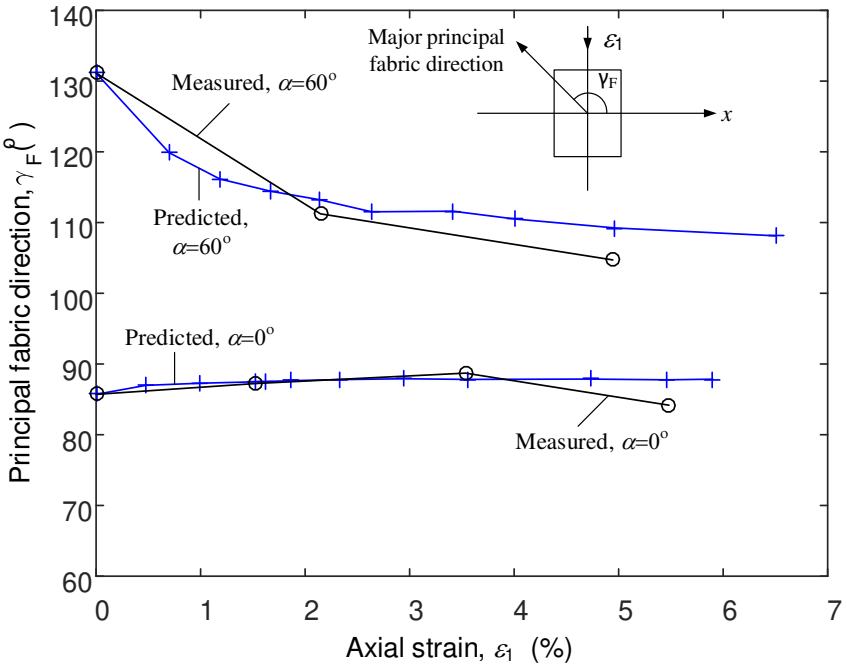

Fig. 7 Measured and predicted evolutions of major principal fabric direction γ_F with axial strain ε_1 for assemblies with different initial fabrics.

7.2. Comparison with tests of Calvetti et al. [3]

Several laboratory tests on 2D material specimens composed of wooden roller stacks were performed by Calvetti et al. [3] to analyse the material behaviour under complex loading conditions, involving loading-unloading cycles and principal axes rotations. It has been shown that the macroscopic behaviour of this 2D material, whose internal friction angle was about 28° (±2°), was qualitatively similar to that of real granular materials (e.g. sands) under loading paths such as compression, shear, and constant volume tests. The fabric tensor, used by Calvetti et al. [3], was normalised by the initial distribution of contact normal and defined by a distribution function of the contact normal truncated by second-order Fourier series. This is similar to Eq. (4). Hence, the evolution of this fabric tensor reflects the underlying mechanisms of evolution of contact normal, and it can be reasonably assumed that the hybrid evolution law is able to capture the evolution of the fabric tensor. The rearrangement anisotropy d, defined by Calvetti et al. [3], can be linked to the fabric deviator F_q by:

$$F_q = \sqrt{2}d \tag{29}$$

As listed in Table 3, results from four different types of tests were used to validate the hybrid evolution law. In summary, during the CHCV1 test (Fig. 8), the specimen was first loaded and

unloaded in horizontal compression under constant vertical stress (part CH), followed by vertical compression under constant horizontal stress (part CV); during the UVUH1 test (Fig. 9), the specimen was first loaded in vertical compression, then unloaded and finally loaded in horizontal compression, keeping the volume constant; the UDUG1 shear test (Fig. 10) was performed under constant volume conditions, in which the boundary strains were imposed controlling the rotation g of the loading device lateral plates; in the CHCD1 test (Fig. 11) the specimen was first loaded in horizontal compression (CH part) and then subjected to right shear (CD part), as the vertical stress was kept constant. The stress and strain control conditions applied in each of the tests are also briefly summarised in Figs. 8-11, respectively. More details of the tests refer to [41].

The measured and predicted evolutions of the fabric tensor, in terms of the fabric deviator and major principal fabric direction, are compared in Figs. 8-11. Overall, a close agreement is shown between theory and tests under complex loading and unloading processes, although slight overpredictions on the fabric deviator are made by the hybrid evolution law for the UVUH1 and UDUG1 tests. One of the advantages of the proposed hybrid evolution law is that the evolution of the distribution of contact normals is attributed to two different mechanisms that are related to the stress rate and the plastic strain rate, respectively. Fig. 8 (a) shows that the trajectory of the fabric deviator was mostly reversible during the loading-unloading cycle from step 3 to step7. In other words, the material response was more elastic-like and the plastic strain rate was very low during the unloading process. Similar features were observed during loading and unloading processes in the UVUH1 and the UDUG1 tests as shown in Figs. 9 and 10. In these processes, the fabric evolutions were mainly related to the stress rate. On the other hand, the strain-rate driven mechanism was triggered and dominated at large shear strains. comparisons in Figs. 9 and 10 indicate that the evolution law is applicable to the undrained conditions featured by the constant volume. In addition, it is shown that the fabric evolution in CHCD1 test, where principal axes rotations were involved, can also be generally captured by the hybrid evolution law using the same set of material parameters.

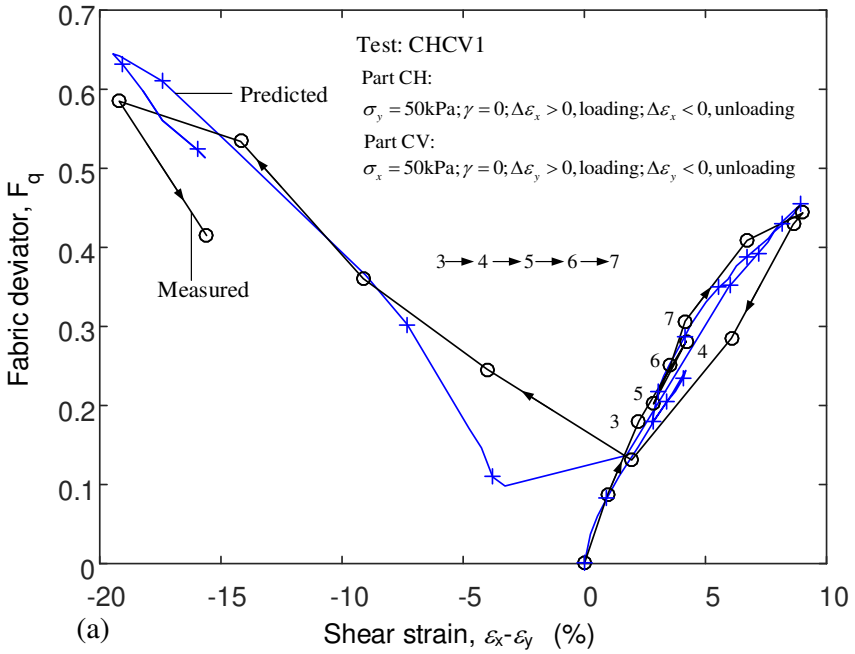

538

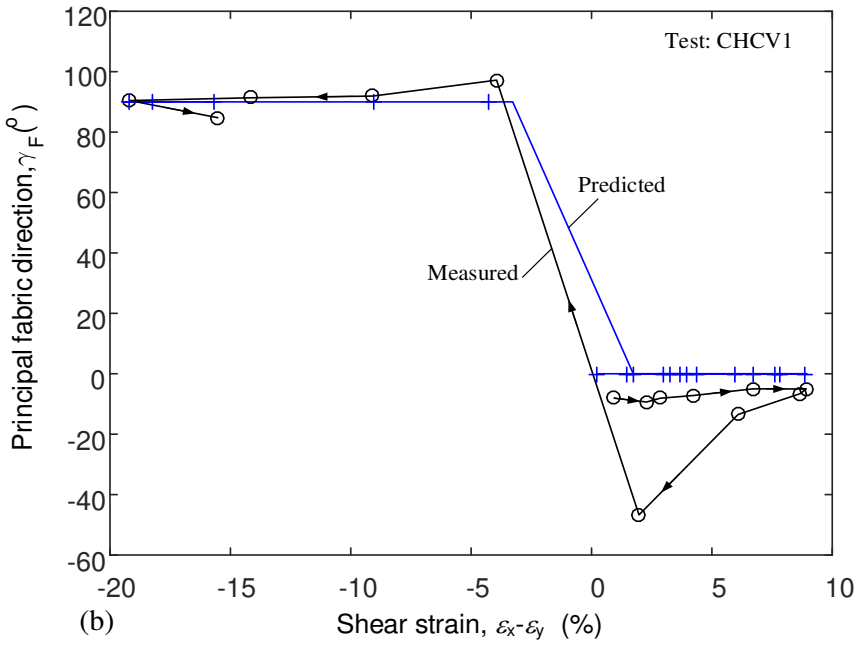

539

540 Fig. 8 Measured and predicted evolutions of fabric tensor against shear strain $\varepsilon_x - \varepsilon_y$ under
541 CHCV1 test: (a) fabric deviator; (b) major principal fabric direction.

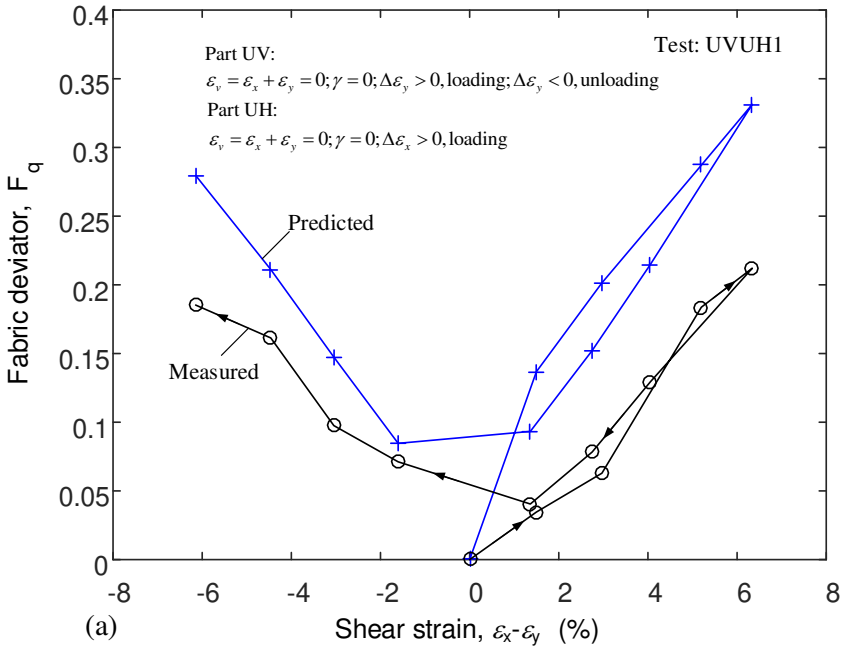

542

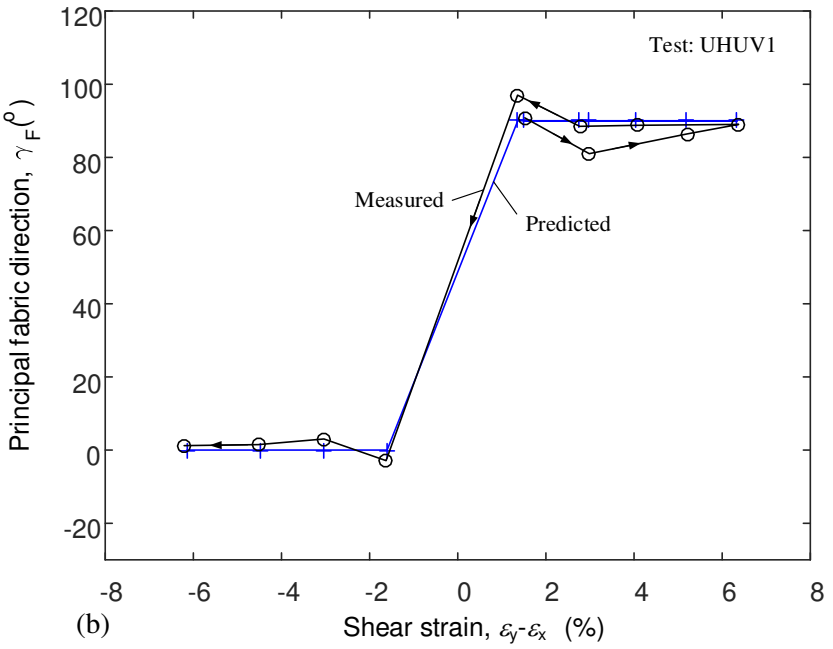

543

544 Fig. 9 Measured and predicted evolutions of fabric tensor against shear strain $\varepsilon_y - \varepsilon_x$ under

545 UVUH1 test: (a) fabric deviator; (b) major principal fabric direction.

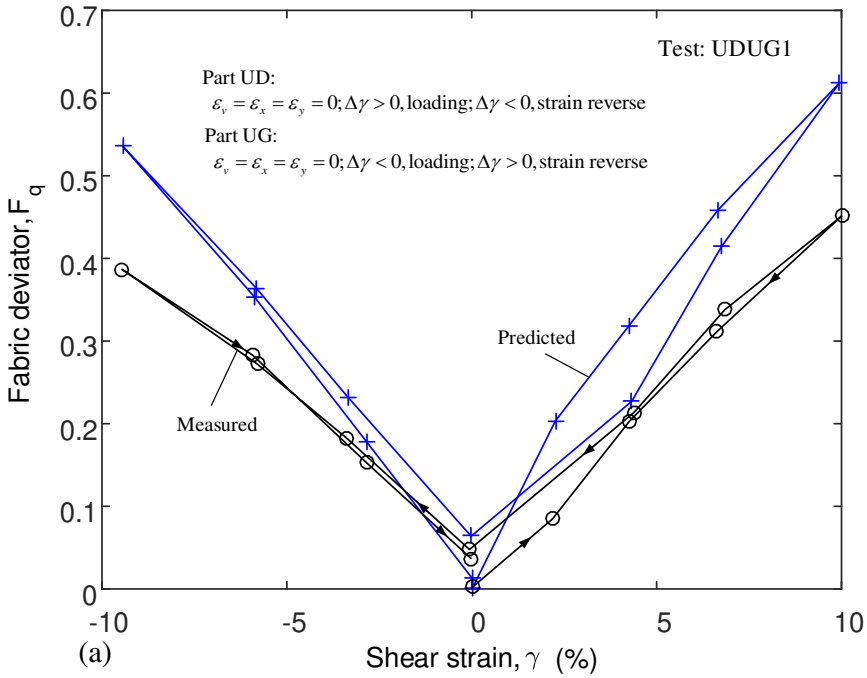

546

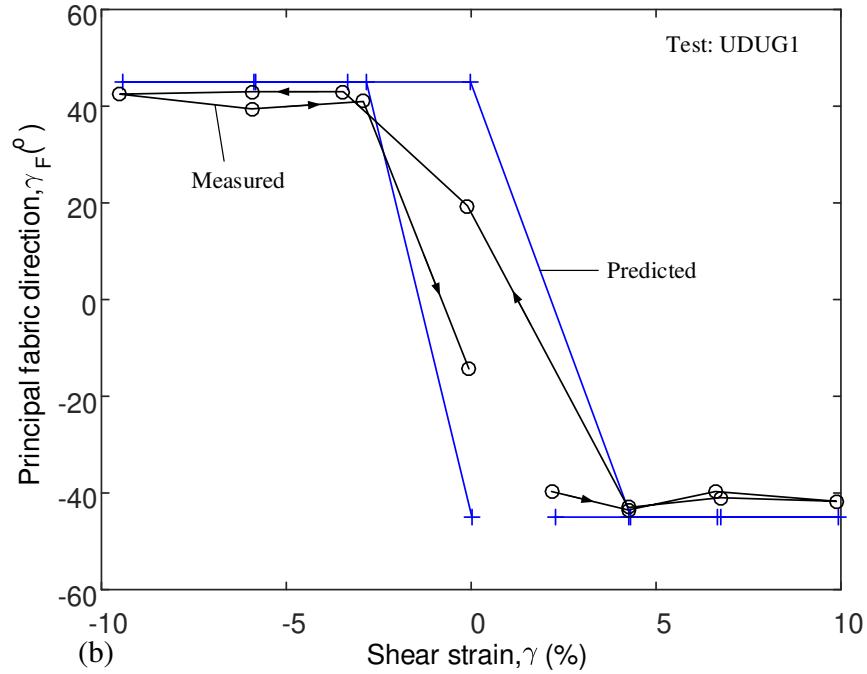

547

548 Fig. 10 Measured and predicted evolutions of fabric tensor against shear strain γ under
549 UDUG1 test: (a) fabric deviator; (b) major principal fabric direction.

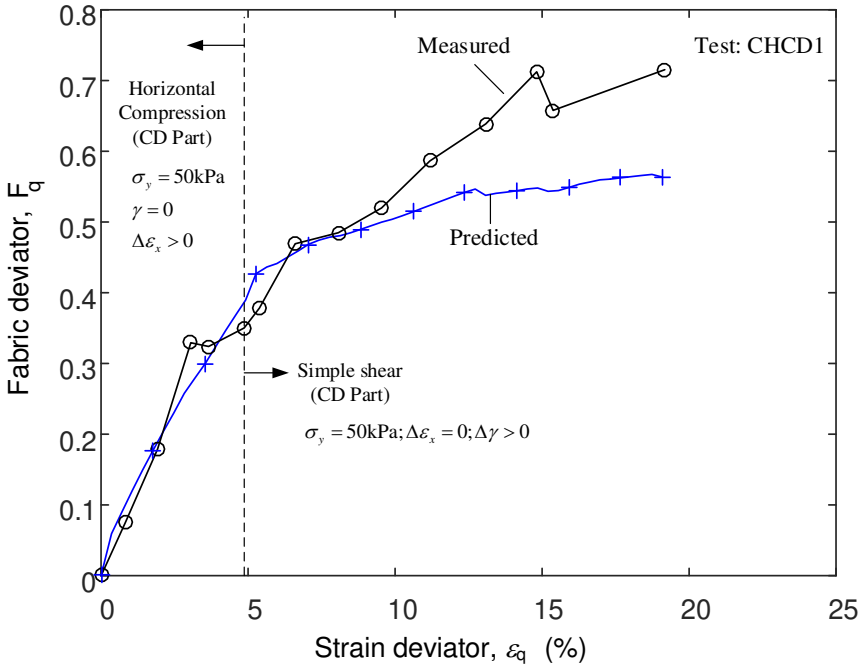

Fig. 11 Measured and predicted evolutions of fabric deviator F_q against strain deviator ε_q under CHCD1 test.

8. Concluding remarks

This paper focuses on the development and assessment of a generic hybrid fabric evolution law for modelling of anisotropic behaviour of granular materials. The evolution law is formulated at the macroscopic level within the general framework of rate-independent elastoplasticity, which is not related to any particular model. Its features and performances are discussed by comparing with DEM simulation results under proportional monotonic shearing and experimental data under complex loading and unloading conditions. The following remarks can be made:

- Evolution laws that assume the rate of the fabric tensor is dependent on stress rate and stress tensor only (e.g. Eq. (9)) violate the uniqueness requirement of the critical state. Strain-rate driven evolution laws in the form of Eq. (21) with an 'attractor' that satisfies Eq. (6c) at the critical state (e.g. Eq. (22)) can ensure a unique critical fabric tensor independent of initial fabric. These two types of evolution laws satisfy the requirements of the principle of material frame-indifference and the assumption of rate-independence.
- Fabric evolution predicted by the hybrid evolution law coincides well with DEM simulations for granular materials under monotonic shearing at various directions. The fabric evolution at low stress ratios is primarily governed by the stress-rate driven term

of the hybrid law, while the strain-rate driven term dominates at high stress ratios and ensures that the fabric tensor evolves towards a unique anisotropic critical state.

- A close agreement between the model predictions and experimental data is shown, which suggests that the hybrid evolution law is also applicable to complex loading conditions involving loading-unloading cycles and rotations of stress axes while the axes rotate by an angle less than 180^{o}.

The accuracy and applicability of the proposed evolutions laws may vary in tests performed under different control conditions (e.g. under purely rotational shearing) [61]. This needs to be further investigated in future studies.

CRediT authorship contribution statement

Nian Hu: Conceptualization, Investigation, Methodology, Writing - original draft, Formal analysis, Validation, Writing - review & editing. **Pei-Zhi Zhuang**: Writing - original draft, Formal analysis, Writing - review & editing, Validation, Funding acquisition, Data Curation. **Dun-Shun Yang**: Validation, Software, Resources, Data Curation. **Hai-Sui Yu**: Conceptualization, Supervision, Funding acquisition, Project administration.

Declaration of Competing Interest

The authors declare that they have no known competing financial interests or personal relationships that could have appeared to influence the work reported in this paper.

Acknowledgements

The authors thank Dr. Xia Li for her help on DEM simulations and the useful discussions on the feature of fabric evolution. The second author would like to acknowledge the funding from the Tai'shan Youth Scholar Program of Shandong Province, China (No. tsqn201909016), the Qilu Scholar Program of Shandong University and the State Key Laboratory for GeoMechanics and Deep Underground Engineering, China University of Mining and Technology (SKLGDUEK1802).

Appendix A.

A monotonic proportional loading path under mixed control is considered. In this specific loading path, the mean effective stress p and the b value are kept constant and the principal

directions of the stress tensor are fixed, while the vertical strain increases gradually. An initially isotropic stress state is assumed for clarity. One example of this type of loading in laboratory tests is the drained constant p triaxial shear test after an isotropic consolidation.

The stress tensor $\boldsymbol{\sigma}$ can be decomposed as:

$$\boldsymbol{\sigma} = p\boldsymbol{I} + \boldsymbol{S} = p\boldsymbol{I} + \lambda\boldsymbol{l} \tag{A 1}$$

where λ and $\boldsymbol{l}$ denote the norm and the direction of the deviatoric stress tensor $\boldsymbol{S}$ respectively.

$$\lambda = \|\boldsymbol{S}\|;\ \ \boldsymbol{l} = \frac{\boldsymbol{S}}{\|\boldsymbol{S}\|};\ \ \|\boldsymbol{l}\| = 1 \tag{A 2}$$

This specific proportional loading can be equivalently described as:

$$\dot{\boldsymbol{l}} = \boldsymbol{0};\ \ \dot{p} = 0 \tag{A 3}$$

Hence, the following relationships can be obtained.

$$\dot{\boldsymbol{S}} = \dot{\lambda}\boldsymbol{l} + \lambda\dot{\boldsymbol{l}} = \dot{\lambda}\boldsymbol{l};\ \ \|\dot{\boldsymbol{S}}\| = |\dot{\lambda}|;\ \ \frac{\dot{\boldsymbol{\sigma}}}{\|\dot{\boldsymbol{\sigma}}\|} = \frac{\dot{\boldsymbol{S}}}{\|\dot{\boldsymbol{S}}\|} = \frac{\dot{\lambda}}{|\dot{\lambda}|}\boldsymbol{l} \tag{A 4}$$

Using the relationships in Eq. (A 4), Eq. (9) reduces to:

$$\dot{\boldsymbol{F}} = \boldsymbol{B}\left(p\boldsymbol{I} + \lambda\boldsymbol{l}, \frac{\dot{\lambda}}{|\dot{\lambda}|}\boldsymbol{l}\right)|\dot{\lambda}| \tag{A 5}$$

Before integrating Eq. (A 5), it is instructive to discuss the stress paths in detail. It can be expected that a sample of granular material, either initially 'dense' or 'loose', will reach the same critical state that is described by Eqs. (6a), (6b) and (6c) at large shear strains, along a such loading path. Note that the critical state stresses for different samples are the same according to Eq. (6b) and hence the critical state fabric tensors should also be identical according to Eq. (6c). In other words, the critical state fabric tensor should be unique under this type of loading irrespective of the initial fabric or density of the sample. Fig. A.1 illustrates the stress paths for both 'dense' and 'loose' samples. Terms 'loose' and 'dense' used here are referred to as whether a peak stress ratio exists. It is well known that for 'loose' samples during a monotonic shearing the stress norm $\lambda = \|\boldsymbol{S}\|$ will increase monotonically from 0 to the critical value $\lambda_c(p)$, along the stress path O-C. While for 'dense' samples, λ will increase up to a peak value $\lambda_p(p)$ due to strain hardening, and then decrease gradually towards the critical value $\lambda_c(p)$ due to strain softening, namely along the path of O-C-P-C.

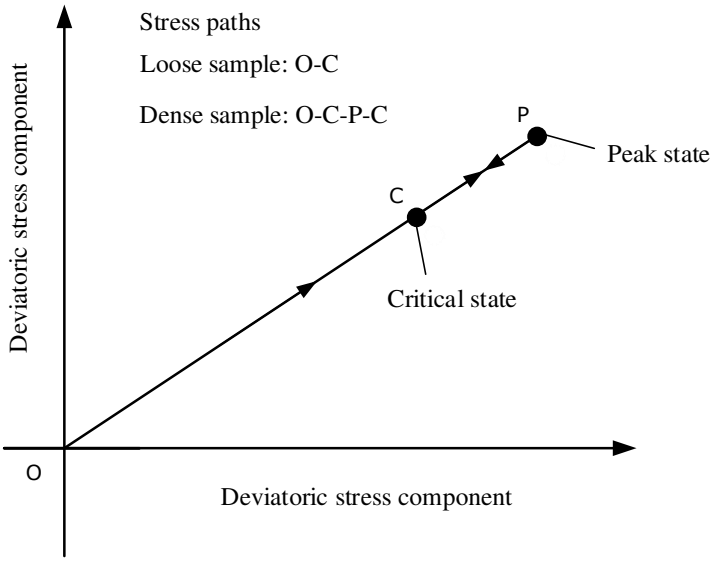

624

625 Figure A.1. Illustration of stress paths in a deviatoric stress space

626 For 'loose' samples, along the stress path O-C there is $\dot{\lambda}/|\dot{\lambda}| = 1$. For 'dense' samples, $\dot{\lambda}/|\dot{\lambda}| =$
627 1 along O-C-P, whereas $\dot{\lambda}/|\dot{\lambda}| = -1$ after the peak strength along the path P-C. Since $|\dot{\lambda}|$
628 approaches zero while reaching the critical state, it can be seen from Eq. (A 5) that the critical
629 fabric tensor will be 'saturated', which means that the fabric tensor will no longer change as
630 the shear strain develops further. Thus, the critical state fabric tensor $\boldsymbol{F_c}$ can be obtained by
631 integrating Eq. (A 5) along the stress path O-C-P-C as:

632 $$\boldsymbol{F}_c - \boldsymbol{F}_i = \int_0^{\lambda_p} \boldsymbol{B}(p\boldsymbol{I} + \lambda\boldsymbol{l}, \boldsymbol{l})\, d\lambda - \int_{\lambda_p}^{\lambda_c} \boldsymbol{B}(p\boldsymbol{I} + \lambda\boldsymbol{l}, -\boldsymbol{l})\, d\lambda \quad \text{(A 6)}$$

633 where $\boldsymbol{F}_i$ is the initial fabric tensor. Rewriting Eq. (A 6) leads to:

634 $$\boldsymbol{F}_c = \boldsymbol{F}_i + \boldsymbol{F}_{c1} + \boldsymbol{F}_{c2} \quad \text{(A 7)}$$

635 $$\boldsymbol{F}_{c1} = \int_0^{\lambda_c} \boldsymbol{B}(p\boldsymbol{I} + \lambda\boldsymbol{l}, \boldsymbol{l})\, d\lambda \quad \text{(A 8)}$$

636 $$\boldsymbol{F}_{c2} = \int_{\lambda_c}^{\lambda_p} \big(\boldsymbol{B}(p\boldsymbol{I} + \lambda\boldsymbol{l}, \boldsymbol{l}) + \boldsymbol{B}(p\boldsymbol{I} + \lambda\boldsymbol{l}, -\boldsymbol{l})\big)\, d\lambda \quad \text{(A 9)}$$

637 Note that the stress direction $\boldsymbol{l}$ remains unchanged in this loading path. The term $\boldsymbol{F}_{c1}$ is the
638 stress-induced fabric tensor along the stress path O-C, and the term $\boldsymbol{F}_{c2}$ is the stress-induced
639 fabric tensor along the stress path C-P-C.

640 Eq. (6b) specifies that the critical state stresses are unique and independent of the initial state.
641 Hence, the stress-induced fabric tensors $\boldsymbol{F}_{c1}$ should be the same for 'loose' and 'dense' samples.

For ‘loose’ samples, there are no peak stress states, i.e. $\lambda_c = \lambda_p$, hence $\boldsymbol{F}_{c2}$ is always zero. Eq. (A 7) shows $\boldsymbol{F}_{\mathrm{c}}$ will not be unique for samples with different initial fabric tensors, dependent on $\boldsymbol{F}_i$ instead, which means that Eqs. (9) and (6c) are not compatible for ‘loose’ samples at the critical state. For ‘dense’ samples, providing that $\boldsymbol{B}$ is an odd function in terms of the stress rate $\dot{\boldsymbol{\sigma}}$, e.g. $\boldsymbol{B}$ is linear with $\dot{\boldsymbol{\sigma}}$ (see Section 3.2), there is $\boldsymbol{B}(p\boldsymbol{I} + \lambda\boldsymbol{l}, -\boldsymbol{l}) = -B(p\boldsymbol{I} + \lambda\boldsymbol{l}, \boldsymbol{l})$, thus $\boldsymbol{F}_{c2} = 0$. This situation is the same as that of ‘loose’ samples. For the case where $\boldsymbol{B}(pI + \lambda\boldsymbol{l}, -\boldsymbol{l}) \neq -\boldsymbol{B}(p\boldsymbol{I} + \lambda\boldsymbol{l}, \boldsymbol{l})$, $\boldsymbol{F}_{c2}$ may vary with the peak strength λ_p which is also dependent on the initial void ratio [84]. Consequently, $\boldsymbol{F}_c$ will not be unique either as both $\boldsymbol{F}_i$ and $\boldsymbol{F}_{c2}$ are dependent on the initial state of the material. Overall, Eqs. (9) and (6c) are not compatible at the critical state for ‘dense’ samples.

References

[1] Fonseca J, O'Sullivan C, Coop MR, Lee P. Quantifying the evolution of soil fabric during shearing using directional parameters. Geotechnique. 2013;63(6):487-99.

[2] Majmudar TS, Behringer RP. Contact force measurements and stress-induced anisotropy in granular materials. Nature. 2005;435(7045):1079-82.

[3] Calvetti F, Combe G, Lanier J. Experimental micromechanical analysis of a 2D granular material: relation between structure evolution and loading path. Mechanics of Cohesive‐frictional Materials: An International Journal on Experiments, Modelling and Computation of Materials and Structures. 1997;2(2):121-63.

[4] Oda M, Nemat-Nasser S, Konishi J. Stress-induced anisotropy in granular masses. Soils and Foundations. 1985;25(3):85-97.

[5] Oda M, Konishi J. Rotation of principal stresses in granular material during simple shear. Soils and Foundations. 1974;14(4):39-53.

[6] Oda M, Konishi J. Microscopic deformation mechanism of granular material in simple shear. Soils and Foundations. 1974;14(4):25-38.

[7] Sun Q, Zheng J, He H, Li Z. Particulate material fabric characterization from volumetric images by computational geometry. Powder Technology. 2019;344:804-13.

[8] Oda M, Takemura T, Takahashi M. Microstructure in shear band observed by microfocus X-ray computed tomography. Geotechnique. 2004;54(8):539-42.

[9] Yuan R, Yu H-S, Yang D-S, Hu N. On a fabric evolution law incorporating the effects of b-value. Computers and Geotechnics. 2019;105:142-54.

[10] Wang R, Dafalias YF, Fu P, Zhang J-M. Fabric evolution and dilatancy within anisotropic critical state theory guided and validated by DEM. International Journal of Solids and Structures. 2019;188–189:210-22.

[11] Shi J, Guo P. Induced fabric anisotropy of granular materials in biaxial tests along imposed strain paths. Soils and Foundations. 2018;58(2):249-63.

678 [12] Yang Z, Wu Y. Critical state for anisotropic granular materials: a discrete element
679 perspective. International Journal of Geomechanics. 2017;17(2):04016054.

680 [13] Zhao J, Guo N. Unique critical state characteristics in granular media considering fabric
681 anisotropy. Geotechnique. 2013;63(8):695-704.

682 [14] Kruyt NP. Micromechanical study of fabric evolution in quasi-static deformation of
683 granular materials. Mechanics of Materials. 2012;44:120-9.

684 [15] Fu P, Dafalias YF. Fabric evolution within shear bands of granular materials and its
685 relation to critical state theory. International Journal for numerical and analytical methods in
686 geomechanics. 2011;35(18):1918-48.

687 [16] Thornton C, Zhang L. On the evolution of stress and microstructure during general 3D
688 deviatoric straining of granular media. Geotechnique. 2010;60(5):333-41.

689 [17] Li X, Yu H-S. Influence of loading direction on the behavior of anisotropic granular
690 materials. International Journal of Engineering Science. 2009;47(11-12):1284-96.

691 [18] Thornton C. Numerical simulations of deviatoric shear deformation of granular media.
692 Geotechnique. 2000;50(1):43-53.

693 [19] Thornton C, Antony S. Quasi–static deformation of particulate media. Philosophical
694 Transactions of the Royal Society of London Series A: Mathematical, Physical and
695 Engineering Sciences. 1998;356(1747):2763-82.

696 [20] Rothenburg L, Bathurst R. Analytical study of induced anisotropy in idealized granular
697 materials. Geotechnique. 1989;39(4):601-14.

698 [21] Cundall PA, Strack OD. A discrete numerical model for granular assemblies.
699 Geotechnique. 1979;29(1):47-65.

700 [22] Sibille L, Hadda N, Nicot F, Tordesillas A, Darve F. Granular plasticity, a contribution
701 from discrete mechanics. Journal of the Mechanics and Physics of Solids. 2015;75:119-39.

702 [23] Li X, Yu H-S. Numerical investigation of granular material behaviour under rotational
703 shear. Geotechnique. 2010;60(5):381-94.

[24] Oda M. Initial fabrics and their relations to mechanical properties of granular material. Soils and Foundations. 1972;12(1):17-36.

[25] Gregory PJ, Nortcliff S. Soil conditions and plant growth: John Wiley & Sons, 2013.

[26] Ouadfel H, Rothenburg L. Stress–force–fabric'relationship for assemblies of ellipsoids. Mechanics of Materials. 2001;33(4):201-21.

[27] Xie Y, Yang Z, Barreto D, Jiang M. The influence of particle geometry and the intermediate stress ratio on the shear behavior of granular materials. Granular Matter. 2017;19(2):35(1-13).

[28] Kruyt NP, Agnolin I, Luding S, Rothenburg L. Micromechanical study of elastic moduli of loose granular materials. Journal of the Mechanics and Physics of Solids. 2010;58(9):1286-301.

[29] Tsutsumi S, Kaneko K. Constitutive response of idealized granular media under the principal stress axes rotation. International Journal of Plasticity. 2008;24(11):1967-89.

[30] Li X, Yu H-S. Particle-scale insight into deformation noncoaxiality of granular materials. International Journal of Geomechanics. 2013;15(4):04014061.

[31] Hu N, Yu H-S, Yang D-S, Zhuang P-Z. Constitutive modelling of granular materials using a contact normal-based fabric tensor. Acta Geotechnica. 2020;15:1125–51.

[32] Li B, Chen L, Gutierrez M. Influence of the intermediate principal stress and principal stress direction on the mechanical behavior of cohesionless soils using the discrete element method. Computers and Geotechnics. 2017;86:52-66.

[33] Wang R, Cao W, Zhang J-M. Dependency of dilatancy ratio on fabric anisotropy in granular materials. Journal of Engineering Mechanics. 2019;145(10):04019076.

[34] Li XS, Dafalias YF. Anisotropic critical state theory: role of fabric. Journal of Engineering Mechanics. 2012;138(3):263-75.

[35] Gao Z, Zhao J, Li XS, Dafalias YF. A critical state sand plasticity model accounting for fabric evolution. International Journal for Numerical and Analytical Methods in Geomechanics. 2014;38(4):370-90.

731 [36] Li X, Yu H, Li X. Macro–micro relations in granular mechanics. International Journal of
732 Solids and Structures. 2009;46(25):4331-41.

733 [37] Tobita Y. Fabric tensors in constitutive equations for granular materials. Soils and
734 Foundations. 1989;29(4):91-104.

735 [38] Wan RG, Guo PJ. Stress dilatancy and fabric dependencies on sand behavior. Journal of
736 Engineering Mechanics. 2004;130(6):635-45.

737 [39] Dafalias YF, Papadimitriou AG, Li XS. Sand plasticity model accounting for inherent
738 fabric anisotropy. Journal of Engineering Mechanics. 2004;130(11):1319-33.

739 [40] Yang Z, Xu T, Chen Y. Unified Modeling of the Influence of Consolidation Conditions
740 on Monotonic Soil Response Considering Fabric Evolution. Journal of Engineering Mechanics.
741 2018;144(8):04018073.

742 [41] Petalas AL, Dafalias YF, Papadimitriou AG. SANISAND-F: Sand constitutive model with
743 evolving fabric anisotropy. International Journal of Solids and Structures. 2019;188-189:12-
744 31.

745 [42] Nemat-Nasser S. A micromechanically-based constitutive model for frictional
746 deformation of granular materials. Journal of the Mechanics and Physics of Solids. 2000;48(6-
747 7):1541-63.

748 [43] Nicot F, Darve F, Group R. A multi-scale approach to granular materials. Mechanics of
749 Materials. 2005;37(9):980-1006.

750 [44] Zhu H, Mehrabadi MM, Massoudi M. Incorporating the effects of fabric in the dilatant
751 double shearing model for planar deformation of granular materials. International Journal of
752 Plasticity. 2006;22(4):628-53.

753 [45] Wang R, Cao W, Xue L, Zhang J-M. An anisotropic plasticity model incorporating fabric
754 evolution for monotonic and cyclic behavior of sand. Acta Geotechnica. 2020(1).

755 [46] Tatsuoka F. Small strain behaviour of granular materials. Mechanics of Granular Materials:
756 an Introduction. 1999:299-308.

[47] Oda M, Konishi J, Nemat-Nasser S. Experimental micromechanical evaluation of strength of granular materials: effects of particle rolling. Mechanics of Materials. 1982;1(4):269-83.

[48] Konishi J, Oda M, Nemat-Nasser S. Inherent anisotropy and shear strength of assembly of oval cross-sectional rods. IUTAM Conference on Deformation and Failure of Granular Materials. Amsterdam, Netherlands: A.A. Balkema, 1982. p. 403–12.

[49] Shi J, Guo P. Fabric evolution of granular materials along imposed stress paths. Acta Geotechnica. 2018;13(6):1341-54.

[50] Yang Z, Wu Y. Critical state for anisotropic granular materials: a discrete element perspective. International Journal of Geomechanics. 2016;17(2):04016054.

[51] Yang D. Microscopic study of granular material behaviours under general stress paths: University of Nottingham, 2014.

[52] Li X, Yu H-S, Li XS. Macro–micro relations in granular mechanics. International Journal of Solids and Structures. 2009;46(25-26):4331-41.

[53] Zhu H, Nguyen HN, Nicot F, Darve F. On a common critical state in localized and diffuse failure modes. Journal of the Mechanics and Physics of Solids. 2016;95:112-31.

[54] Jiang M, Li T, Shen Z. Fabric rates of elliptical particle assembly in monotonic and cyclic simple shear tests: a numerical study. Granular Matter. 2016;18(3):54(1-14).

[55] Yu H-S. Non-coaxial theories of plasticity for granular materials. The 12th International Conference of International Association for Computer Methods and Advances in Geomechanics (IACMAG). Goa, India: Citeseer, 2008. p. 361-77.

[56] Zhu H, Mehrabadi MM, Massoudi M. Three-dimensional constitutive relations for granular materials based on the dilatant double shearing mechanism and the concept of fabric. International Journal of Plasticity. 2006;22(5):826-57.

[57] Rothenburg L, Kruyt NP. Critical state and evolution of coordination number in simulated granular materials. International Journal of Solids and Structures. 2004;41(21):5763-74.

[58] Sun J, Sundaresan S. A constitutive model with microstructure evolution for flow of rate-independent granular materials. Journal of Fluid Mechanics. 2011;682:590-616.

[59] Zhao C, Kruyt NP. An evolution law for fabric anisotropy and its application in micromechanical modelling of granular materials. International Journal of Solids and Structures. 2020;196-197:53-66.

[60] Wang R, Dafalias YF, Fu P, Zhang J-M. Fabric evolution and dilatancy within anisotropic critical state theory guided and validated by DEM. International Journal of Solids and Structures. 2020;188–189:210-22.

[61] Hu N. On Fabric Tensor-based Constitutive Modelling of Granular Materials: Theory and Numerical Implementation. Nottingham, UK: University of Nottingham, 2015.

[62] Fu P, Dafalias YF. Relationship between void-and contact normal-based fabric tensors for 2D idealized granular materials. International Journal of Solids and Structures. 2015;63:68-81.

[63] Kanatani K-I. Distribution of directional data and fabric tensors. International Journal of Engineering Science. 1984;22(2):149-64.

[64] Li X, Yu H-S. On the stress–force–fabric relationship for granular materials. International Journal of Solids and Structures. 2013;50(9):1285-302.

[65] Satake M. Fabric tensor in granular materials. IUTAM Conference on Deformation and Failure of Granular Materials. Amsterdam, Netherlands: A.A. Balkema, 1982. p. 63-8.

[66] Been K, Jefferies M, Hachey J. The critical state of sands. Geotechnique. 1991;41(3):365-81.

[67] Wood DM. Soil behaviour and critical state soil mechanics. Cambridge, UK: Cambridge University Press, 1990.

[68] Sitharam T, Vinod JS. Critical state behaviour of granular materials from isotropic and rebounded paths: DEM simulations. Granular Matter. 2009;11(1):33-42.

[69] Theocharis AI, Vairaktaris E, Dafalias YF, Papadimitriou AG. Necessary and sufficient conditions for reaching and maintaining critical state. International Journal for Numerical and Analytical Methods in Geomechanics. 2019;43:2041-55.

[70] Dafalias YF. Must critical state theory be revisited to include fabric effects? Acta Geotechnica. 2016;11(3):479-91.

811 [71] Wang R, Fu P, Zhang J-M, Dafalias YF. Evolution of various fabric tensors for granular
812 media toward the critical state. Journal of Engineering Mechanics. 2017;143(10):04017117.

813 [72] Fu P, Dafalias YF. Study of anisotropic shear strength of granular materials using DEM
814 simulation. International Journal for Numerical and Analytical Methods in Geomechanics.
815 2011;35(10):1098-126.

816 [73] Gurtin ME, Fried E, Anand L. The mechanics and thermodynamics of continua.
817 Cambridge, UK: Cambridge University Press, 2009.

818 [74] Wang C-C. A new representation theorem for isotropic functions: An answer to Professor
819 GF Smith's criticism of my papers on representations for isotropic functions. Archive for
820 Rational Mechanics and Analysis. 1970;36(3):166-97.

821 [75] Chaboche J-L. A review of some plasticity and viscoplasticity constitutive theories.
822 International Journal of Plasticity. 2008;24(10):1642-93.

823 [76] Taiebat M, Dafalias YF. SANISAND: Simple anisotropic sand plasticity model.
824 International Journal for Numerical and Analytical Methods in Geomechanics.
825 2008;32(8):915-48.

826 [77] Hashiguchi K. Description of inherent/induced anisotropy of soils: Rotational hardening
827 rule with objectivity. Soils and Foundations. 2001;41(6):139-45.

828 [78] Sekiguchi H, Ohta K. Induced anisotropy and time dependency in clays. In: Murayama S,
829 Schofield AN, editors. Proceeding 9th Intemational Conference on Soil Mechanics and
830 Foundation Engineering, Specialty Session 9. Tokyo1977. p. 229-38.

831 [79] Ma X, Zhang DZ. Statistics of particle interactions in dense granular material under
832 uniaxial compression. Journal of the Mechanics and Physics of Solids. 2006;54(7):1426-48.

833 [80] Kuhn MR. Micro-mechanics of fabric and failure in granular materials. Mechanics of
834 Materials. 2010;42(9):827-40.

835 [81] Lai Y, Liao M, Hu K. A constitutive model of frozen saline sandy soil based on energy
836 dissipation theory. International Journal of Plasticity. 2016;78:84-113.

[82] Li X, Yang D, Yu HS. Macro deformation and micro structure of 3D granular assemblies subjected to rotation of principal stress axes. Granular Matter. 2016;18(3).

[83] Oda M, Konishi J, Nemat-Nasser S. Some experimentally based fundamental results on the mechanical behaviour of granular materials. Geotechnique. 1980;30(4):479-95.

[84] Bolton MD. The strength and dilatancy of sands. Geotechnique. 1986;36(1):65-78.